Journal of Magnetic Resonance **143,** 45–68 (2000)
doi:10.1006/jmre.1999.1980, available online at http://www.idealibrary.com on IDEAL®

Cross-Correlated Relaxation for the Measurement of Angles between Tensorial Interactions

Bernd Reif,[1] Alexander Diener, Mirko Hennig,[2] Marcus Maurer, and Christian Griesinger[3]

Institut für Organische Chemie, Universität Frankfurt, Marie-Curie-Strasse 11, D-60439 Frankfurt, Germany

Received May 25, 1999; revised October 18, 1999

Theory, experimental aspects, and use in structure calculation of cross-correlated relaxation rates measured on zero- and double-quantum coherences in liquid state NMR are presented. The relative size of the interaction depends on the projection angle between the two tensorial interactions. The tensorial interaction can be either a dipolar interaction or a chemical shift anisotropy relaxation mechanism (CSA). Effects of additional sources of relaxation on the cross-correlated relaxation rates are analyzed. Also, an easy-to-use formalism is given to manipulate different cross-correlated relaxation interactions. The application addresses measurement of the backbone angle ψ in a protein by measuring dipole(^{15}N–^{1}H)–dipole($^{13}C^{\alpha}$–$^{1}H^{\alpha}$) and CSA(^{15}N)–dipole($^{13}C^{\alpha}$–$^{1}H^{\alpha}$) cross-correlated relaxation rates. It is shown that ambiguities due to the 3 $\cos^2\theta$-1 dependence of one cross-correlated relaxation rate can be overcome by measuring additional cross-correlated relaxation rates. The use of cross-correlated relaxation rates is demonstrated in structure calculations. © 2000 Academic Press

INTRODUCTION

Recently, we introduced a new structural parameter into high-resolution NMR that uses cross-correlated relaxation of double- and zero-quantum coherences to extract structural information (*1*). The parameter allows the measurement of projections of tensorial interactions onto each other. As opposed to NMR of liquids, such projections of tensors have been determined and interpreted in structural terms in solid-state *local field separated* (*2*), spin diffusion (*3*), or multiple-quantum NMR spectroscopy (*4*). For the last approach, the orientation of the two tensors with respect to each other can be derived from the sideband pattern of the multiple quantum coherences. In NMR of liquids, however, magnetic interactions between two tensors of rank 2 which belong to different heteronuclei can only be measured via double- and zero-quantum coherences and detected through relaxation. The main source of relaxation is the dipolar interaction between directly bound nuclei. In two pairs of nuclei (A^1–A^2 and B^1–B^2), projection angle dependent cross-correlated relaxation rates due to two dipolar couplings $\Gamma^{c}_{A^1A^2,B^1B^2}$ of double- and zero-quantum coherences between nuclei A^1 and B^1 can be measured provided the following requirements are fulfilled:

(a) The desired double- and zero-quantum coherence between nuclei A^1 and B^1 can be excited.

(b) There are couplings such that antiphase coherences between A^1 and A^2 as well as between B^1 and B^2 can be refocused.

(c) The main relaxation source for single-quantum coherence of A^1 (SQC) is the dipolar coupling to A^2 and the main relaxation source of SQC of B^1 is the dipolar coupling to B^2.

The dipole tensor between two spins A^1 and A^2 (B^1 and B^2) is axially symmetric with the axis of symmetry collinear to the bond defined as the internuclear vector $\mathbf{A^1A^2}$. The structural implication of the angular dependence of the interaction of two dipole tensors $\mathbf{A^1A^2}$ and $\mathbf{B^1B^2}$ is therefore straightforward. It directly defines the interbond angle. For cross-correlated relaxation rates involving chemical shift anisotropy (CSA), the CSA tensor needs to be determined in the molecular frame either experimentally or by quantum chemical calculations. The latter requirement is not always fulfilled and makes the measurement of dipolar cross-correlated relaxation rates easier to interpret from a structure point of view.

To further illustrate the principle of the cross-correlated relaxation, we assume that we have two pairs of vectors A^1–A^2 and B^1–B^2 spanning an angle θ. We now describe the effects of cross-correlated relaxation on the lineshape and line intensities of double-quantum (DQ) or zero-quantum (ZQ) coherence with active nuclei A^1 and B^1 (Fig. 1).

These DQ and ZQ coherences evolve chemical shift $\Omega_{A^1} + \Omega_{B^1}$ and $\Omega_{A^1} - \Omega_{B^1}$, respectively. A doublet of doublet of lines is generated with splittings due to scalar coupling of $J(A^1, A^2)$ and $J(B^1, B^2)$ if A^2 and B^2 are not decoupled during this indirect evolution period. We further assume that the sign of the gyromagnetic ratios of A^1 and A^2 and the signs of the two coupling constants are positive. In the absence of cross-corre-

[1] Present address: Institut für Organische Chemie und Biochemie, Tu München, Lichtenbegstr4 D-85747 Garching, Germany.

[2] Present address: The Scripps Research Institute, 10550 North Torrey Pines Road, La Jolla, CA 92037.

[3] Also: Max Planck Institute für Biophysikalische Chemie, Am Faßberg11, 37077 Göttingen, Germany.

1090-7807/00 $35.00
Copyright © 2000 by Academic Press
All rights of reproduction in any form reserved.

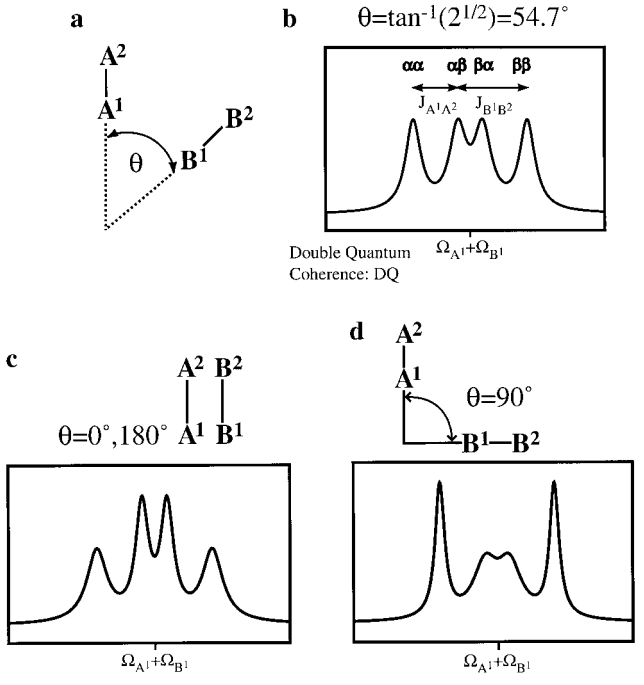

FIG. 1. (a) Cross-correlated relaxation of double- and zero-quantum coherences: The requirement imposed on the spin system is that there are two pairs A^1–A^2 and B^1–B^2. The couplings $J(A^1, A^2)$ and $J(B^1, B^2)$ must be resolved. In addition, the dipolar relaxation A^1–A^2 and B^1–B^2 should be the main source of T_2 relaxation of A^1 and B^1, respectively. (b–d) Schematic multiplet pattern observed for intervectorial angles of $\theta = 54.6°$, 180°, and 90°. The cross correlation of relaxation leads to different linewidths for the multiplet components.

lated relaxation, all four multiplet components would have the same linewidth and intensities (Fig. 1b). α and β denote the polarization of A^1 and A^2, respectively. Including the effects of cross-correlated relaxation, the relative intensities of the lines are different depending on the relative orientation of the two vectors. If the two vectors A^1–A^2 and B^1–B^2 are oriented parallel to each other, the outer two lines are broader than the inner lines (Fig. 1c). The opposite is true for orthogonal orientation of the two vectors (Fig. 1d). Equal intensity for all four lines is also obtained if the two vectors span the *magic angle* $\theta = \tan^{-1}(\sqrt{2}) \approx 54.7°$ (Fig. 1b).

Cross-correlated relaxation has already been used in the past in high-resolution NMR as well. Dalvit and Bodenhausen (*5*) introduced in 1988 a triple-quantum-filtered NOESY for single-quantum coherences only where a system of three nuclei, H_α, $H_\beta^{\text{pro-R}}$, and $H_\beta^{\text{pro-S}}$, in a protein is investigated to yield structural information about the side chain conformation. The complementary experiment applicable for biomacromolecules is the triple-quantum-filtered ROESY, published by Brüschweiler *et al.* (*6*) in 1989. The drawback of the two experiments is their inherently low sensitivity which is due to the large distances of the spins involved. Furthermore, the experiments can only be carried out if the involved nuclei are scalar coupled. Quantitative interpretation of the spectra with respect to the size of the involved angle $\theta_{kl,km}$ is very difficult since the multiplets are affected by scalar couplings and relaxation, which are difficult to disentangle.

Vold *et al.* (*7*) have shown on dilute solutions of trisubstituted benzenes such as 1,2,3-trichlorobenzene that cross-correlation rates can also be used to determine the motional anisotropy of a molecule. Since the rate R_1 for each individual line is a function of the corresponding spectral density for the transition between the respective spin states (*8*), D_{xx}, D_{yy}, and D_{zz} can be estimated after calculation of the transition probabilities for a AB_2 spin system—assuming a nonspherical reorientational process.

Another experiment that has been recorded to characterize hindered or unhindered rotation of side chains in a protein (χ_1) was introduced by Ernst and Ernst (*9*) in 1994. Sign changes in the cross-correlation rate are interpreted as a function of the motional model of the side chain. However, all these approaches did not provide structural information in a simple way.

In the following, a mathematical description of the effect of dipole–dipole and dipole–CSA cross-correlated relaxation in solution NMR will be given.

THEORETICAL DESCRIPTION

Cross-Correlated Relaxation of Zero- and Double-Quantum Coherences

In the following, we consider two spin pairs, a N–H^N vector and a C^α–H^α vector in a protein, for which we excite double- and zero-quantum coherences between N and C^α. The equation of motion for the different components of double-quantum and zero-quantum coherences $\hat{\sigma}_{\mu,\mu'}^{\text{DQ/ZQ}}$ under the influence of the scalar coupled, directly bound, protons has the general form

$$(\hat{\sigma}_{\mu,\mu'}^{\text{DQ/ZQ}})^{\cdot} = [-\hat{\hat{\Gamma}}^{\text{DQ/ZQ}} - i\Omega^{\text{DQ/ZQ}}](\hat{\sigma}_{\mu,\mu'}^{\text{DQ/ZQ}}). \qquad [1]$$

The terms $\hat{\sigma}_{\mu,\mu'}^{\text{DQ/ZQ}}$ summarize the double- and zero-quantum coherences $C^+N^+H_C^\mu H_N^{\mu'}$, $C^-N^-H_C^\mu H_N^{\mu'}$, $C^+N^-H_C^\mu H_N^{\mu'}$, and $C^-N^+H_C^\mu H_N^{\mu'}$. $H_C^\mu H_N^{\mu'}$ ($\mu, \mu' = \alpha, \beta$) stands for the spin polarization operators of the nitrogen- and carbon-bound protons, respectively. The isotropic chemical shift $\Omega^{\text{DQ/ZQ}}$ (the index DQ refers to coherences C^+N^+, ZQ to coherences C^+N^-; for the hermitian conjugate coherences C^-N^- and C^-N^+, all signs in Eq. [2] are inverted) for the four resonance lines with $(\mu, \mu') = (\alpha\alpha)$, $(\alpha\beta)$, $(\beta\alpha)$, and $(\beta\beta)$ of the doublet of doublets is given by

$$\Omega^{\mathrm{DQ/ZQ}} = \left[(\Omega_{\mathrm{C}} \pm \Omega_{\mathrm{N}})1 + \pi \begin{pmatrix} \pm J_{\mathrm{NH}} + J_{\mathrm{CH}} & 0 & 0 & 0 \\ 0 & \mp J_{\mathrm{NH}} + J_{\mathrm{CH}} & 0 & 0 \\ 0 & 0 & \pm J_{\mathrm{NH}} - J_{\mathrm{CH}} & 0 \\ 0 & 0 & 0 & \mp J_{\mathrm{NH}} - J_{\mathrm{CH}} \end{pmatrix} \right]. \quad [2]$$

Ω_{C} and Ω_{N} are the carbon and nitrogen chemical shifts and ${}^1J_{\mathrm{NH}}$ and ${}^1J_{\mathrm{CH}}$ the relative chemical shifts of the different multiplet lines due to the scalar coupling. The relaxation matrix $\hat{\hat{\Gamma}}^{DQ/ZQ}$ has the form

$$\hat{\hat{\Gamma}}^{\mathrm{DQ/ZQ}} = \begin{pmatrix} \Gamma^{\mathrm{a}} + \Gamma_1 + \Gamma_{\alpha\alpha}^{\mathrm{DQ/ZQ}} & -\Gamma_{T1}(\mathrm{H^N}) & -\Gamma_{T1}(\mathrm{H^C}) & -W_2 \\ -\Gamma_{T1}(\mathrm{H^N}) & \Gamma^{\mathrm{a}} + \Gamma_1 + \Gamma_{\alpha\beta}^{\mathrm{DQ/ZQ}} & -W_0 & -\Gamma_{T1}(\mathrm{H^C}) \\ -\Gamma_{T1}(\mathrm{H^C}) & -W_0 & \Gamma^{\mathrm{a}} + \Gamma_1 + \Gamma_{\beta\alpha}^{\mathrm{DQ/ZQ}} & -\Gamma_{T1}(\mathrm{H^N}) \\ -W_2 & -\Gamma_{T1}(\mathrm{H^C}) & -\Gamma_{T1}(\mathrm{H^N}) & \Gamma^{\mathrm{a}} + \Gamma_1 + \Gamma_{\beta\beta}^{\mathrm{DQ/ZQ}} \end{pmatrix}$$

$$\Gamma_1 = \Gamma_{T1}(\mathrm{H^N}) + \Gamma_{T1}(\mathrm{H^C}). \quad [3]$$

In the relaxation matrix $\hat{\hat{\Gamma}}^{\mathrm{DQ/ZQ}}$, the term $\Gamma_{\mu,\mu'}^{\mathrm{DQ/ZQ}}$ denotes the different cross-relaxation rates due to the heteronuclear dipolar interaction, including the dipole–dipole cross-relaxation rate $\Gamma^{\mathrm{c}}_{\mathrm{NH,CH}}$, the CSA–dipole cross-relaxation rates $\Gamma^{\mathrm{c}}_{\mathrm{C,NH}}$, $\Gamma^{\mathrm{c}}_{\mathrm{N,NH}}$, $\Gamma^{\mathrm{c}}_{\mathrm{C,CH}}$, and $\Gamma^{\mathrm{c}}_{\mathrm{N,CH}}$, and the secular part of the relaxation of double-quantum and zero-quantum transitions due to NOE between the protons $\mathrm{H^N}$ and $\mathrm{H^C}$, W_2 and W_0. The nonsecular part of the latter mechanism is reflected in the off-diagonal elements W_2 and W_0. Γ^{a} contains the contributions due to autocorrelated relaxation and external relaxation of C, N-DQ/ZQ coherences. $\Gamma_{T1}(\mathrm{H^N})$ and $\Gamma_{T1}(\mathrm{H^C})$ denote the contributions due to T_1 relaxation of the proton directly attached to the carbon and nitrogen, respectively. The influence of nonsecular contributions in the relaxation matrix $\hat{\hat{\Gamma}}^{\mathrm{DQ/ZQ}}$ on the angle-dependent dipole–dipole cross-relaxation rate is discussed in detail later in this article. Secular contributions in $\hat{\hat{\Gamma}}^{\mathrm{DQ/ZQ}}$ are discussed in the following.

Dipole–Dipole Cross-Correlated Relaxation

In the following, we focus on the relaxation due to the heteronuclear dipolar couplings. The relaxation superoperator in Eq. [A.6] which acts on double- and zero-quantum coherences contains contributions from autocorrelated relaxation ($V = W =$ dipole NH or dipole CH),

$$[\hat{\hat{\Gamma}}^{\mathrm{a}}_{\mathrm{NH,NH}} + \hat{\hat{\Gamma}}^{\mathrm{a}}_{\mathrm{CH,CH}}](\hat{\sigma}^{\mathrm{DQ/ZQ}}_{\mu,\mu'}) = b^2_{\mathrm{NH}} \sum_{q=-2}^{2} [\hat{A}^{(-q)}_{\mathrm{NH}}, [\hat{A}^{(q)}_{\mathrm{NH}}, \hat{\sigma}^{\mathrm{DQ/ZQ}}_{\mu,\mu'}]]\, j^{q}_{\mathrm{NH,NH}}(\omega_q) + b^2_{\mathrm{CH}} \sum_{q=-2}^{2} [\hat{A}^{(-q)}_{\mathrm{CH}}, [\hat{A}^{(q)}_{\mathrm{CH}}, \hat{\sigma}^{\mathrm{DQ/ZQ}}_{\mu,\mu'}]]\, j^{q}_{\mathrm{CH,CH}}(\omega_q), \quad [4]$$

and from cross-correlated relaxation ($V \neq W$),

$$[\hat{\hat{\Gamma}}^{\mathrm{c}}_{\mathrm{NH,CH}} + \hat{\hat{\Gamma}}^{\mathrm{c}}_{\mathrm{CH,NH}}](\hat{\sigma}^{\mathrm{DQ/ZQ}}_{\mu,\mu'}) = b_{\mathrm{NH}} b_{\mathrm{CH}} \sum_{q=-2}^{2} [\hat{A}^{(-q)}_{\mathrm{NH}}, [\hat{A}^{(q)}_{\mathrm{CH}}, \hat{\sigma}^{\mathrm{DQ/ZQ}}_{\mu,\mu'}]]\, j^{q}_{\mathrm{NH,CH}}(\omega_q) + b_{\mathrm{NH}} b_{\mathrm{CH}} \sum_{q=-2}^{2} [\hat{A}^{(-q)}_{\mathrm{CH}}, [\hat{A}^{(q)}_{\mathrm{NH}}, \hat{\sigma}^{\mathrm{DQ/ZQ}}_{\mu,\mu'}]]\, j^{q}_{\mathrm{CH,NH}}(\omega_q), \quad [5]$$

in which $V = \mathrm{NH}$ and $W = \mathrm{CH}$. In the autocorrelation case, the relaxation superoperator contains second-rank tensor operators stemming from only one interaction, whereas in the cross-correlated case, double commutators containing tensor operators from two distinct interactions have to be evaluated. In the secular approximation, only double commutators with a Larmor frequency of 0 contribute (*vide infra*). The terms b_{NH} and b_{CH} are given in Eq. [A.1]. The expressions for the different relaxation rates for auto- and cross-correlated relaxation shall be illustrated in the following. As an example, the double commutator from Eqs. [4] and [5] is applied to double-quantum coherences $\mathrm{C^+N^+H^{\mu}_C H^{\mu'}_N}$. For clarity, the operator symbols on the proton, carbon, and nitrogen operators are omitted in the following. The complementary expressions $\mathrm{C^-N^-H^{\mu}_C H^{\mu'}_N}$ and zero-quantum coherences behave accordingly. The four terms $\mathrm{C^+N^+H^{\mu}_C H^{\mu'}_N}$ ($\mu, \mu' = \alpha, \beta$) corresponding to the four multiplet lines of the doublet of doublets are subjected to the different double commutators for auto- and cross-correlated relaxation. This is summarized in Fig. 2. Note that the result of the double commutators differs only in sign due to the relation $\mathrm{H_z H^{\alpha}} = \frac{1}{2}\mathrm{H^{\alpha}}$ and $\mathrm{H_z H^{\beta}} = -\frac{1}{2}\mathrm{H^{\beta}}$. Note that the gyromagnetic ratio of N

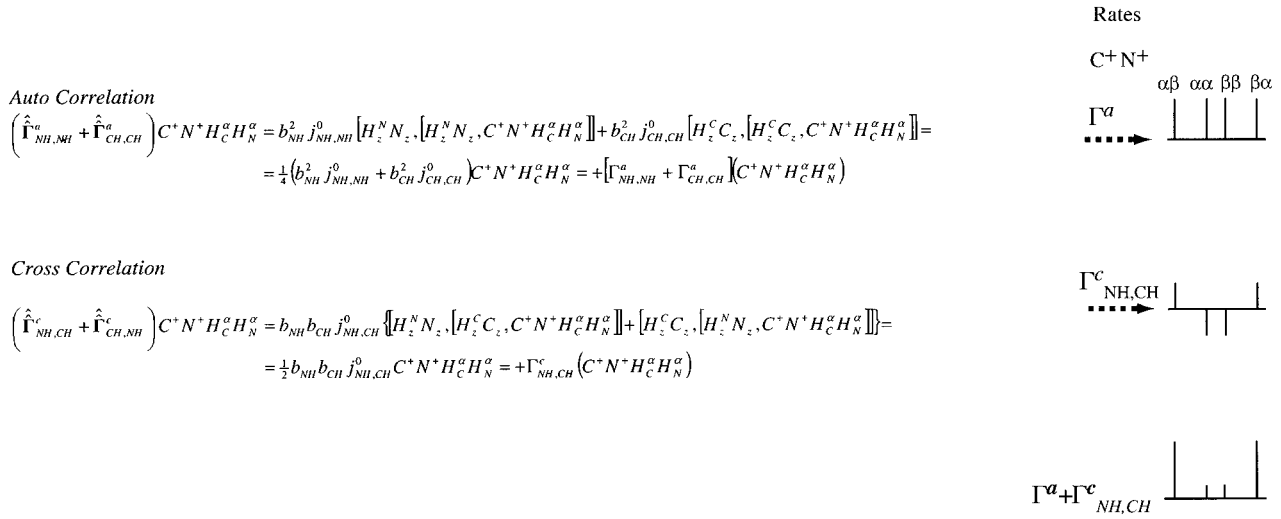

FIG. 2. Double commutators for dipole–dipole auto- and cross-correlated relaxation and respective rates in a graphical representation.

and the ^{1}J(N,H) coupling constant are both assumed to be negative.

In the autocorrelated case, as well as in the cross-correlated case, the *single line operators* $C^{+}N^{+}H^{\mu}_{C}H^{\mu'}_{N}$ are eigenoperators with respect to the $j^{0}(0)$ part. In the autocorrelated case, all lines relax equally fast, whereas in the cross-correlated case, for the two pairs of lines $\alpha\alpha$ and $\beta\beta$, as well as $\alpha\beta$ and $\beta\alpha$, the rates have the same absolute value, but opposite sign. The right-hand side of Fig. 2 shows a graphical representation of the respective rates. Altogether, the multiplet is governed by a superposition of the rates of Γ^{a} and $\Gamma^{c}_{NH,CH}$, which is indicated by the sum of the two rates at the bottom at the right-hand side of Fig. 2.

For the simplest case of isotropic reorientation, the dipole–dipole cross-correlated relaxation rate for each multiplet line of the doublet of doublets according to Eq. [5], with the spectral density function given in Eq. [A.8] for a spherical top molecule, can be written as

$$\Gamma^{c}_{NH,CH}=\frac{\gamma_H\gamma_N}{(r_{NH})^3}\frac{\gamma_H\gamma_C}{(r_{CH})^3}\left(\frac{\mu_0}{4\pi}\hbar\right)^2\frac{1}{5}(3\cos^2\theta_{NH,CH}-1)\tau_c. \qquad [6]$$

Thereby, $\theta_{NH,CH}$ denotes the projection angle between the NH and the CH vector.

Dipole–CSA Cross-Correlated Relaxation

The cross-correlated relaxation between a dipolar coupling and a CSA tensor, e.g., dipole(NH) with CSA(N) or dipole(NH) with CSA(C), contributes to the relaxation rates of the four resonance lines. The rates for the CSA–dipole cross-correlated relaxation are derived from Eq. [A.6]. A double commutator for cross-correlated relaxation between CSA(^{13}C) and a dipolar coupling of N–H is given as an example in Fig. 3. Note that the cross-correlated relaxation rates for the four lines differ only in sign but not in absolute value. Therefore, they can be summarized as shown in Fig. 3. Note that the assignment of the order of the spin polar-

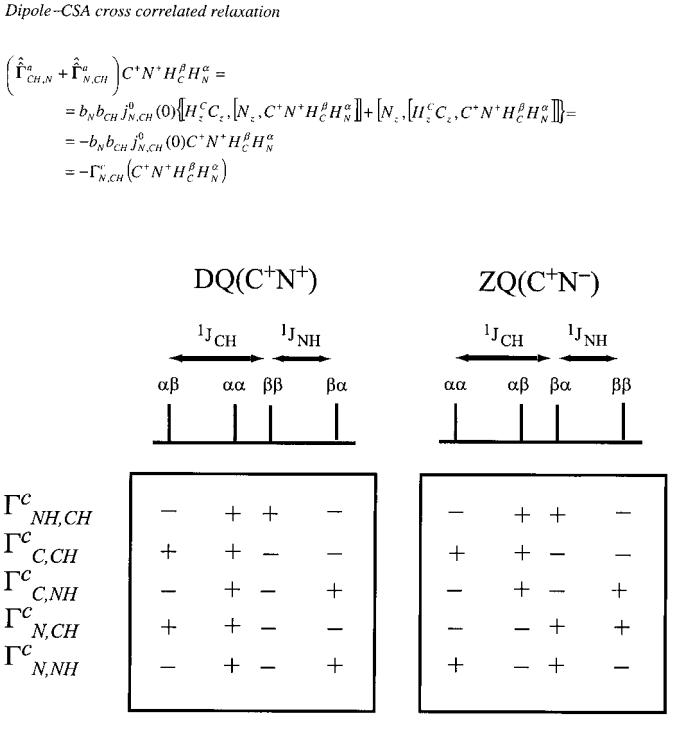

FIG. 3. Schematic representation of the dipole–CSA cross-correlated relaxation rates of C, N DQ and ZQ coherences. The double commutator serves as an example. The sign of the rates for the respective submultiplet line is given in the boxes.

ization states of the multiplet components differs between DQ and ZQ coherences.

For the double-quantum operator, the sums of the rates of the cross-correlated spectral densities for CSA(^{13}C) and CSA(^{15}N) with dipole NH and CH, respectively, are observed. Accordingly, for the respective zero-quantum coherences, the difference of the rates will be observed which allows us to determine each rate individually, as will be shown later. According to Eq. [5], together with Eqs. [A.2], [A.3], [A.4], and Eq. [A.8], the general form for the dipole–CSA cross-correlated relaxation rate can be written as for isotropic tumbling,

$$\Gamma^{c}_{N,CH} = -\frac{2}{15}\gamma_N B_0 \tau_c \hbar \frac{\mu_0}{4\pi}\frac{\gamma_H\gamma_C}{(r_{CH})^3} \times \{(\sigma_{xx}-\sigma_{zz})(3\cos^2\theta_{CH,\sigma_{xx}}-1) + (\sigma_{yy}-\sigma_{zz})(3\cos^2\theta_{CH,\sigma_{yy}}-1)\}, \quad [7a]$$

where $\theta_{CH,\sigma_{xx}}$ and $\theta_{CH,\sigma_{yy}}$ denote the angle between the CH vector and the two principal components of the nitrogen CSA tensor. An equivalent formulation is

$$\Gamma^{c}_{N,CH} = -\frac{2}{15}\gamma_N B_0 \tau_c \hbar \frac{\mu_0}{4\pi}\frac{\gamma_H\gamma_C}{(r_{CH})^3} \times \left\{(\sigma_\parallel-\sigma_\perp)(3\cos^2\theta_{CH,\sigma_\parallel}-1) + \frac{3}{4}(\sigma_{xx}-\sigma_{yy})(\sin^2\theta_{CH,\sigma\parallel}\cos 2\phi_{CH,\sigma_{xx}})\right\}. \quad [7b]$$

If the CSA tensor is axially symmetric, Eq. [7b] simplifies accordingly, setting $\sigma_{xx} = \sigma_{yy} = \sigma_\perp$ and $\sigma_{zz} = \sigma_\parallel$:

$$\Gamma^{c}_{N,CH} = -\frac{2}{15}\gamma_N B_0 \tau_c \hbar \frac{\mu_0}{4\pi}\frac{\gamma_H\gamma_C}{(r_{CH})^3} \times \{(\sigma_\parallel-\sigma_\perp)(3\cos^2\theta_{CH,\sigma_\parallel}-1)\}. \quad [7c]$$

Further Relaxation Contributions

The cross-correlated relaxation rates affect the different multiplet components differently. Therefore, other relaxation rates that behave similarly must be investigated as well. The NOE between the two protons H^N and H^C leads to different relaxation rates of the $\alpha\alpha$ and $\beta\beta$ lines compared to the $\alpha\beta$ and $\beta\alpha$ lines. A quantification of the size of this effect is given in this subsection. The NOE between the two protons H^N and H^C stems from the $j^{(0)}(\omega_{HC}-\omega_{HN})$ $[W_0]$ and the $j^{(2)}(\omega_{HC}+\omega_{HN})$ $[W_2]$ term of the autocorrelated dipolar relaxation between the two protons. The respective double commutators for W_0 are

$$\begin{aligned}(C^+N^+H_C^\alpha H_N^\beta)^\cdot &= -b^2_{H^CH^N} j^{(0)}(\omega_{H^C}-\omega_{H^N})[-\tfrac{1}{4}(H_C^+H_N^- + H_C^-H_N^+),\\ &\quad [-\tfrac{1}{4}(H_C^+H_N^- + H_C^-H_N^+), C^+N^+H_C^\alpha H_N^\beta]]\\ &= -\tfrac{1}{8} b^2_{H^CH^N} j^{(0)}(\omega_{H^C}-\omega_{H^N})(H_C^\alpha H_N^\beta - H_C^\beta H_N^\alpha)C^+N^+\\ &= W_0(H_C^\alpha H_N^\beta - H_C^\beta H_N^\alpha)C^+N^+ \end{aligned} \quad [8a]$$

and similarly for $(C^+N^+H_C^\beta H_N^\alpha)^\cdot$. The respective double commutators for W_2 can be written as

$$\begin{aligned}(C^+N^+H_N^\alpha H_C^\alpha)^\cdot &= -b^2_{H^CH^N} j^{(2)}(\omega_{H^C}+\omega_{H^N})\\ &\quad \times\{[\sqrt{\tfrac{3}{8}}H_C^+H_N^+, [\sqrt{\tfrac{3}{8}}H_C^-H_N^-, C^+N^+H_N^\alpha H_C^\alpha]]\\ &\quad + [\sqrt{\tfrac{3}{8}}H_C^-H_N^-, [\sqrt{\tfrac{3}{8}}H_C^+H_N^+, C^+N^+H_N^\alpha H_C^\alpha]]\}\\ &= -\tfrac{3}{4} b^2_{H^CH^N} j^{(2)}(\omega_{H^C}+\omega_{H^N})\{(H_C^\alpha H_N^\alpha - H_C^\beta H_N^\beta)C^+N^+\}\\ &= -W_2(H_C^\alpha H_N^\alpha - H_C^\beta H_N^\beta)C^+N^+ \end{aligned} \quad [8b]$$

and similarly for $(C^+N^+H_C^\beta H_N^\beta)^\cdot$. Thus, the contribution to the full relaxation matrix due to NOE is given by

$$\begin{pmatrix}\sigma_{\alpha\alpha}^{DQ/ZQ}\\ \sigma_{\alpha\beta}^{DQ/ZQ}\\ \sigma_{\beta\alpha}^{DQ/ZQ}\\ \sigma_{\beta\beta}^{DQ/ZQ}\end{pmatrix}^\cdot = -\begin{pmatrix}+W_2 & 0 & 0 & -W_2\\ 0 & +W_0 & -W_0 & 0\\ 0 & -W_0 & +W_0 & 0\\ -W_2 & 0 & 0 & +W_2\end{pmatrix}\begin{pmatrix}\sigma_{\alpha\alpha}^{DQ/ZQ}\\ \sigma_{\alpha\beta}^{DQ/ZQ}\\ \sigma_{\beta\alpha}^{DQ/ZQ}\\ \sigma_{\beta\beta}^{DQ/ZQ}\end{pmatrix}. \quad [9]$$

The NOE contributes a secular and a nonsecular term. We will see in the following that the nonsecular term can be ignored. However, the secular term remains and contributes to the linewidth of the $\alpha\alpha$, $\beta\beta$ line the rate W_2 and to the $\alpha\beta$, $\beta\alpha$ line the rate W_0. This must be taken into account in the simulations carried out for the evaluation of the dipole–dipole cross-correlated relaxation rate $\Gamma^c_{NH,CH}$ in the following section.

Practical Extraction Procedure

The relative signs of the relaxation rates of the individual lines $\alpha\alpha$, $\alpha\beta$, $\beta\alpha$, and $\beta\beta$ can be written—as stated above—in the secular approximation as follows for the DQ spectrum,

$$\Gamma^{DQ}_{\alpha\alpha} = +\Gamma^{a} + \Gamma^{c}_{NH,CH} + \Gamma^{c}_{N,NH} + \Gamma^{c}_{C,NH} + \Gamma^{c}_{N,CH} + \Gamma^{c}_{C,CH} + W_2 + \Gamma_1$$

$$\Gamma^{DQ}_{\alpha\beta} = +\Gamma^{a} - \Gamma^{c}_{NH,CH} - \Gamma^{c}_{N,NH} - \Gamma^{c}_{C,NH} + \Gamma^{c}_{N,CH} + \Gamma^{c}_{C,CH} + W_0 + \Gamma_1$$

$$\Gamma^{DQ}_{\beta\alpha} = +\Gamma^{a} - \Gamma^{c}_{NH,CH} + \Gamma^{c}_{N,NH} + \Gamma^{c}_{C,NH} - \Gamma^{c}_{N,CH} - \Gamma^{c}_{C,CH} + W_0 + \Gamma_1$$

$$\Gamma^{DQ}_{\beta\beta} = +\Gamma^{a} + \Gamma^{c}_{NH,CH} - \Gamma^{c}_{N,NH} - \Gamma^{c}_{C,NH} - \Gamma^{c}_{N,CH} - \Gamma^{c}_{C,CH} + W_2 + \Gamma_1, \quad [10a]$$

and the ZQ spectrum,

$$\Gamma^{ZQ}_{\alpha\alpha} = +\Gamma^{a} - \Gamma^{c}_{NH,CH} + \Gamma^{c}_{N,NH} - \Gamma^{c}_{C,NH} - \Gamma^{c}_{N,CH} + \Gamma^{c}_{C,CH} + W_0 + \Gamma_1$$

$$\Gamma^{ZQ}_{\alpha\beta} = +\Gamma^{a} + \Gamma^{c}_{NH,CH} - \Gamma^{c}_{N,NH} + \Gamma^{c}_{C,NH} - \Gamma^{c}_{N,CH} + \Gamma^{c}_{C,CH} + W_2 + \Gamma_1$$

$$\Gamma^{ZQ}_{\beta\alpha} = +\Gamma^{a} + \Gamma^{c}_{NH,CH} + \Gamma^{c}_{N,NH} - \Gamma^{c}_{C,NH} + \Gamma^{c}_{N,CH} - \Gamma^{c}_{C,CH} + W_2 + \Gamma_1$$

$$\Gamma^{ZQ}_{\beta\beta} = +\Gamma^{a} - \Gamma^{c}_{NH,CH} - \Gamma^{c}_{N,NH} + \Gamma^{c}_{C,NH} + \Gamma^{c}_{N,CH} - \Gamma^{c}_{C,CH} + W_0 + \Gamma_1. \quad [10b]$$

The relaxation rate of a signal is reflected in the linewidth at half height. In the experiment described below, double- and zero-quantum coherences are evolved in a *constant time* manner during the time T. The relaxation rate of each multiplet component is directly reflected in the intensity of the signal by $I_{\mu\nu} \propto \exp(-\Gamma_{\mu\nu}T)$. Correspondingly, the cross-correlated relaxation rates can be extracted from the multiplet intensities and also the integrals according to

$$\Gamma^{c,DQ}_{NH,CH} = \frac{1}{4T}\ln\left(\frac{I^{DQ}(\alpha\beta)\, I^{DQ}(\beta\alpha)}{I^{DQ}(\alpha\alpha)\, I^{DQ}(\beta\beta)}\right) - \frac{1}{2}(W_2 - W_0)$$

$$\Gamma^{c,ZQ}_{NH,CH} = \frac{1}{4T}\ln\left(\frac{I^{ZQ}(\alpha\alpha)\, I^{ZQ}(\beta\beta)}{I^{ZQ}(\alpha\beta)\, I^{ZQ}(\beta\alpha)}\right) - \frac{1}{2}(W_2 - W_0). \quad [11]$$

Note that the reliability can be checked by variation of the constant time delay T (*10*). Note that this implies always taking the product of the intensities of the inner lines in the nominator and the product of the intensities of the outer lines in the denominator of the logarithm (Fig. 3).

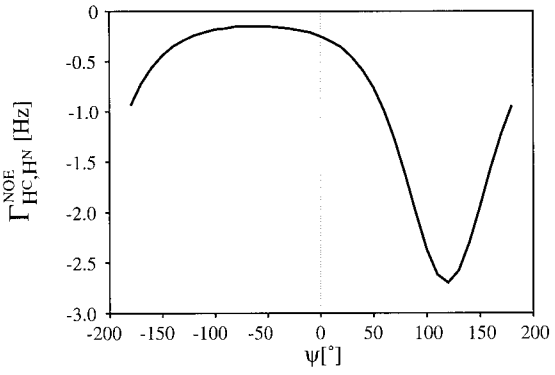

FIG. 4. NOE cross-correlation rate $\Gamma^{NOE}_{H^C,H^N}$ between the protons H^{α}_{k} and H^{N}_{k+1} in a protein as a function of the peptide backbone angle ψ (τ_c = 6.4 ns) according to Eq. [12]. ψ is correlated with the distance between the two protons by the relation given in Fig. 11b.

We have calculated the dipole–dipole cross-correlated relaxation rate on the left-hand side of Eq. [11] with simulations with the program WTEST (*11*). The basis for these simulations are Eqs. [4] and [5]. To obtain the angular information about the included projection angle between the bond vectors N–H^N and C^{α}–H^{α}, Eq. [6], which describes the angular dependence of the dipole–dipole cross-correlation rate, is combined with Eq. [11].

The contribution to the dipole–dipole cross-correlated relaxation rate due to NOE between the two protons is given by the difference of the rates W_2 and W_0 which are given by (*12*, *13*)

$$W_0 = \frac{1}{10}\left(\frac{\mu_0}{4\pi}\right)^2\left(\frac{\hbar\gamma_H^2}{r^3_{H^CH^N}}\right)^2\tau_c \quad [12a]$$

$$W_2 = \frac{1}{10}\left(\frac{\mu_0}{4\pi}\right)^2\left(\frac{\hbar\gamma_H^2}{r^3_{H^CH^N}}\right)^2\tau_c\left[\frac{6}{1+4(\omega_H\tau_c)^2}\right]. \quad [12b]$$

To get an impression of the size of the effect, Fig. 4 shows the cross-correlation rate $\Gamma^{NOE}_{H^C,H^N} = W_2 - W_0$ between the two protons H^{α}_{k} and H^{N}_{k+1} in a protein as a function of the backbone angle ψ. The overall correlation time τ_c was assumed to be 6.4 ns.

The four cross-correlated relaxation rates $\Gamma^{c}_{N,NH}$, $\Gamma^{c}_{C,NH}$, $\Gamma^{c}_{N,CH}$, and $\Gamma^{c}_{C,CH}$ can be extracted from Eq. [10] in a similar way as the dipole–dipole cross-correlated relaxation rates $\Gamma^{c}_{NH,CH}$ were obtained. The single dipole(NH)–CSA cross-correlation rates are given by

$$\Gamma^{c}_{N,NH} = \frac{1}{8T} \times \ln\left(\frac{I^{DQ}(\alpha\beta)\, I^{DQ}(\beta\beta)\, I^{ZQ}(\alpha\beta)\, I^{ZQ}(\beta\beta)}{I^{DQ}(\alpha\alpha)\, I^{DQ}(\beta\alpha)\, I^{ZQ}(\alpha\alpha)\, I^{ZQ}(\beta\alpha)}\right)$$

$$\Gamma^{c}_{N,CH} = \frac{1}{8T} \times \ln\left(\frac{I^{DQ}(\alpha\beta)\, I^{DQ}(\beta\beta)}{I^{DQ}(\alpha\alpha)\, I^{DQ}(\beta\alpha)} \frac{I^{ZQ}(\alpha\alpha)\, I^{ZQ}(\beta\alpha)}{I^{ZQ}(\alpha\beta)\, I^{ZQ}(\beta\beta)}\right) \quad [13]$$

and are similar for the dipole(CH)–CSA cross-correlated relaxation rate,

$$\Gamma^{c}_{C,CH} = \frac{1}{8T} \times \ln\left(\frac{I^{DQ}(\beta\beta)\, I^{DQ}(\beta\alpha)}{I^{DQ}(\alpha\alpha)\, I^{DQ}(\alpha\beta)} \frac{I^{ZQ}(\beta\beta)\, I^{ZQ}(\beta\alpha)}{I^{ZQ}(\alpha\alpha)\, I^{ZQ}(\alpha\beta)}\right)$$

$$\Gamma^{c}_{N,CH} = \frac{1}{8T} \times \ln\left(\frac{I^{DQ}(\beta\beta)\, I^{DQ}(\beta\alpha)}{I^{DQ}(\alpha\alpha)\, I^{DQ}(\alpha\beta)} \frac{I^{ZQ}(\alpha\alpha)\, I^{ZQ}(\alpha\beta)}{I^{ZQ}(\beta\beta)\, I^{ZQ}(\beta\alpha)}\right). \quad [14]$$

The orientation and size of CSA tensors are well known from solid-state NMR studies for amides (*14*) and for aliphatic carbons (*15*) and can be used for these studies in high-resolution NMR. A review of investigations of CSA tensors of all kinds of heteronuclei that have been determined by means of solid-state NMR is given in Ref. (*16*).

As average values for the main components of the ^{15}N CSA tensor for a peptide, one finds in the literature (*16*) $\sigma_{11} = (223 \pm 7)$ ppm, $\sigma_{22} = (79 \pm 8)$ ppm, $\sigma_{33} = (55 \pm 9)$ ppm, and therefore $\Delta\sigma = \sigma_{\parallel} - \sigma_{\perp} = 156$ ppm. The orientation of the ^{15}N CSA tensor is indicated in Fig. 5. The ^{13}C CSA tensor for aliphatic carbons shows only small anisotropy values. One finds the following values for L-threonine (*15*): $\sigma_{11} = (69.0 \pm 0.4)$ ppm, $\sigma_{22} = (58.9 \pm 0.4)$ ppm, and $\sigma_{33} = (52.6 \pm 0.3)$ ppm. Other amino acids have been investigated in Ref. (*17*) showing that the CSA of the $^{13}C_{\alpha}$ varies quite strongly. Therefore DQ and ZQ spectra should show different rates with respect to the scalar $^{1}J_{CH}$ coupling depending on the ψ angle.

Cross-correlated relaxation between C^{α} CSA and ^{15}N CSA does not affect the extraction procedure provided the rates are extracted from DQ and ZQ spectra individually. This holds because this cross-correlated relaxation affects all the submultiplet lines in the same way.

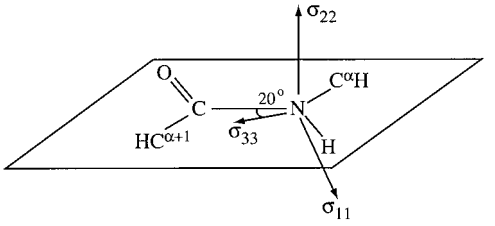

FIG. 5. Orientation of the ^{15}N CSA tensor in a peptide according to Ref. (*14a*). σ_{11} and σ_{33} are oriented in the peptide plane, where σ_{33} is rotated about ca. 20° relative to the C′N bond. σ_{22} is oriented orthogonal to the peptide plane. For an amide nitrogen, σ_{11} is the most shielded component of the CSA tensors.

Constant time versus real time evolution. Cross-correlated relaxation rates can be extracted most easily from *constant time* data since the intensities and the integrals directly reflect the relaxation rates. Under *real time* evolution, this is no longer true and the relaxation rates have to be deconvoluted from a potentially complicated lineshape that is often not known since it includes, e.g., small long-range coupling constants. We propose here a deconvolution procedure that is robust against any underlying lineshape. If we consider a multiplet with four lines with an arbitrary, however, constant lineshape $L(\omega)$ for all multiplet components on top of the Lorentzian lineshape as described by Eq. [10], the Fourier transformation including an apodization function $w(t)$ will yield the following lineshape $F_{\mu\nu}(\omega)$ for the multiplet line $I_{\mu\nu}$:

$$F_{\mu\nu}(\omega) = L(\omega) \otimes \mathrm{FT}[\exp(-\Gamma_{\mu\nu}t)] \otimes FT[w(t)], \quad [15]$$

where $\otimes$ represents convolution.

As described before, the desired cross-correlated relaxation rate can be extracted from

$$\Gamma^{c}_{NH,CH} + \tfrac{1}{2}(W_2 - W_0) = \tfrac{1}{4}(\Gamma_{\alpha\alpha} + \Gamma_{\beta\beta} - \Gamma_{\alpha\beta} - \Gamma_{\beta\alpha}). \quad [16]$$

The difference of the rates of the multiplet components, e.g., $\Gamma_{\alpha\beta} - \Gamma_{\alpha\alpha}$, can be obtained by fitting the lineshape $F_{\alpha\alpha}(\omega)$ to the lineshape $F_{\alpha\beta}(\omega)$ by convolution of the $\alpha\alpha$ multiplet component with a Lorentzian with a trial linewidth $(\Gamma_{\alpha\beta} - \Gamma_{\alpha\alpha})^{trial}$. The best fit for $(\Gamma_{\alpha\beta} - \Gamma_{\alpha\alpha})^{trial}$ and similarly $(\Gamma_{\beta\alpha} - \Gamma_{\beta\beta})^{trial}$ yields the desired cross-correlated relaxation rate. An example on the application of this technique is shown in Fig. 6 (*18*). The $\alpha\alpha$ line is broader than the $\alpha\beta$ line. Duplication of the doublet, shifting one to the low-field side (L) by J and convoluting the high-field multiplet with a trial Lorentzian $L(\omega, LB)$ with the linewidth LB yields the three multiplets of Fig. 6H. The intensities of the $\alpha\alpha(L)$ line and the $\alpha\beta(H)$ line are identical if $LB = (\Gamma_{\alpha\alpha} - \Gamma_{\alpha\beta})$. Figure 6 shows the result of the fitting. The optimal LB is 1.6 Hz.

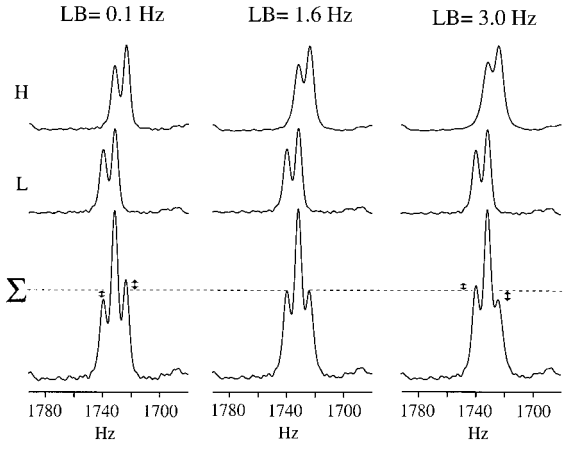

FIG. 6. Extraction procedure for the determination of dipole–dipole cross-correlated relaxation rates from real time data. The two lines under investigation are shifted by the coupling constant that needs to be known. This yields the two multiplets H and L. Exponential broadening is applied on the H doublet and the intensities of the high-field line of the H doublet is compared to the low-field line of the low-field doublet. When they match trace Σ the difference in the linewidth of the two components is determined.

Nonsecular Terms in the DQ/ZQ Relaxation Matrix

To be able to evaluate properly the effect of cross-correlated relaxation, it is necessary that the involved scalar couplings are resolved. However, the resolved couplings also ensure that the relaxation matrix in Eq. [3] is faithfully evaluated taking into account only the secular components. Therefore, spectral density functions of nonzero frequency $j^q(\omega \neq 0)$, proton T_1 relaxation, and proton–proton NOE that introduce nonsecular terms in the DQ/ZQ relaxation matrix $\hat{\hat{\Gamma}}^{\mathrm{DQ/ZQ}}$ can be ignored. These terms lead to coherence transfer between the multiplet components. We show here the influence of these terms which eventually limits the applicability of the method to molecules which are very large by NMR standards where the heteronuclear ^1J couplings are no longer resolved (Fig. 7).

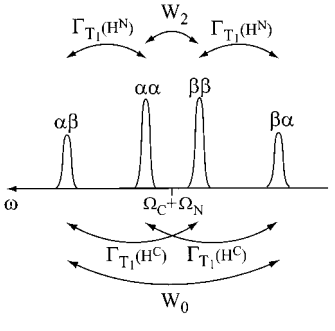

FIG. 7. Schematic representation of the $\alpha\alpha$, $\alpha\beta$, $\beta\alpha$, and $\beta\beta$ multiplet components in a doublet of doublets. Undesired transitions due to NOE between H^N and H^C and T_1 relaxation of the two H^N and H^C protons which correspond to the off-diagonal elements in Eq. [3]. This leads to a transfer of magnetization between the multiplet components as indicated in the figure and to a change in intensities which is considered in the text.

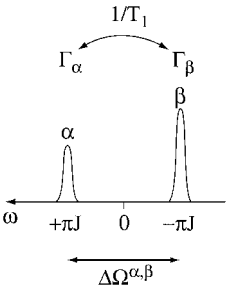

FIG. 8. Schematic representation of a signal which is split due to a scalar coupling of the size $2\pi J$ into a doublet. T_1 relaxation leads to an averaging of signal intensity on the α and the β line and therefore to a downscaling of the cross-correlated relaxation rate $\Gamma^c = |\lambda_1 - \lambda_2|$, as derived from Eq. [22].

a. Contributions to the cross-correlated relaxation rate $\Gamma^c_{NH,CH}$ due to spectral density functions of higher order. In Eq. [5], only double commutators have been considered so far with Larmor frequency $\omega = 0$ for the relaxation of the operators $\sigma^{\mathrm{DQ/ZQ}}_{\mu,\mu'}$. We show here that additional contributions due to other spectral density functions either do not exist or contribute only nonsecular relaxation terms. Except for the $\hat{A}^{(\pm 1)}_{\mathrm{NH}}$, $\hat{A}^{(\mp 1)}_{\mathrm{CH}}$ terms with the C and N operators being longitudinal $\sqrt{\frac{3}{8}}\,\mathrm{N}_z\mathrm{H}^{\pm}_{\mathrm{N}}$ and $\sqrt{\frac{3}{8}}\,\mathrm{C}_z\mathrm{H}^{\pm}_{\mathrm{N}}$, there are no further contributions due to incompatible Larmor frequency in the rotating frame. Evaluation of one of the four possible permutations of the double commutator yields

$$(\mathrm{C}^+\mathrm{N}^+)^{\cdot} = -b_{\mathrm{NH}}b_{\mathrm{CH}}[\sqrt{\tfrac{3}{8}}\,\mathrm{H}^+_{\mathrm{N}}\mathrm{N}_z, [\sqrt{\tfrac{3}{8}}\,\mathrm{H}^-_{\mathrm{C}}\mathrm{C}_z, \mathrm{C}^+\mathrm{N}^+]] \times j^1_{\mathrm{NH,CH}}(\omega_{\mathrm{H}}) = -\Gamma^{c,q=1}_{\mathrm{NH,CH}}(\mathrm{H}^-_{\mathrm{C}}\mathrm{H}^+_{\mathrm{N}}\mathrm{C}^+\mathrm{N}^+). \quad [17]$$

This term is a nonsecular term, provided that the chemical shifts of the two involved protons are different. We show for this example that this relaxation channel does not have any effect on the cross-correlated relaxation rate $\Gamma^c_{\mathrm{NH,CH}}$. The subset of operators connected in the Liouville–von Neumann differential equation by the double commutator of Eq. [17] is given in Eq. [18]. The differential equation describes a transition between the lines of $\mathrm{C}^+\mathrm{N}^+$ and $\mathrm{C}^+\mathrm{N}^+\mathrm{H}^+_{\mathrm{N}}\mathrm{H}^-_{\mathrm{C}}$,

$$\begin{pmatrix} \mathrm{C}^+\mathrm{N}^+ \\ \mathrm{C}^+\mathrm{N}^+\mathrm{H}^+_{\mathrm{N}}\mathrm{H}^-_{\mathrm{C}} \end{pmatrix}^{\cdot} = \begin{pmatrix} 0 & \Gamma \\ \Gamma & i(\Omega_{\mathrm{H^N}} - \Omega_{\mathrm{H^C}}) \end{pmatrix} \times \begin{pmatrix} \mathrm{C}^+\mathrm{N}^+ \\ \mathrm{C}^+\mathrm{N}^+\mathrm{H}^+_{\mathrm{N}}\mathrm{H}^-_{\mathrm{C}} \end{pmatrix}. \quad [18]$$

The Γ terms in the matrix expression of Eq. [18] are obtained after evaluation of the double commutator from Eq. [16]. The relative chemical shift of $\mathrm{C}^+\mathrm{N}^+$ and $\mathrm{C}^+\mathrm{N}^+\mathrm{H}^+_{\mathrm{N}}\mathrm{H}^-_{\mathrm{C}}$ is given by 0 and $\Delta\Omega = \Omega_{\mathrm{H^N}} - \Omega_{\mathrm{H^C}}$, respectively. The eigenvalues λ_1, λ_2 of the matrix are

$$\lambda_{1/2} = i\frac{\Delta\Omega}{2} \pm \sqrt{-\frac{(\Delta\Omega)^2}{4} + \Gamma^2} \overset{\Delta\Omega \gg \Gamma}{\approx} i\frac{\Delta\Omega}{2} \times \left[1 \pm \left(1 - \frac{2\Gamma^2}{\Delta\Omega^2}\right)\right]$$

$$\lambda_1 \approx i\Delta\Omega$$

$$\lambda_2 \approx i\frac{\Gamma^2}{\Delta\Omega}. \qquad [19]$$

It is obvious that for $\Gamma < \Delta\Omega/2$ both eigenvalues are purely imaginary. This is fulfilled for H^C and H^N due to their large difference in chemical shifts. Therefore, as long as this inequality holds, there is no contribution to the linewidths of the doublet of doublets of C^+N^+, but only a contribution to the relative chemical shift originating from double commutators of higher order.

b. Proton T_1 relaxation. In addition, scalar relaxation of the second kind (*19, 20*) due to longitudinal eigenrelaxation (ρ_{ii}- and ρ_{jj}-element of the Redfield matrix) through the interaction of the two involved protons i and j with other nuclei contributes nonsecular elements to the relaxation matrix $\hat{\hat{\Gamma}}^{DQ}$ of Eq. [3] in addition to the equal secular contributions for all lines. T_1 relaxation equilibrates the intensities of the α-line and β-multiplet line of a given doublet which can lead to an underestimation of the angular-dependent cross-correlation rate (Fig. 8). This shall be discussed in this section.

To evaluate the contribution due to T_1 relaxation, it is sufficient to consider here a resonance line which is split due to a scalar coupling in a α- and a β-multiplet component. Their respective relaxation rates shall be Γ_α, Γ_β and their relative chemical shifts $\pm\pi J$. The rates Γ_α and Γ_β contain all the secular contributions. Furthermore, intensity is transferred from the α-line to the β-line by means of T_1 relaxation leading to exchange of coherence between the α- and β-line with the rate $1/T_1$. The system can therefore be described as

$$\begin{pmatrix}\hat{I}^\alpha \\ \hat{I}^\beta\end{pmatrix}^{\cdot} = -\hat{\hat{\Gamma}}\begin{pmatrix}\hat{I}^\alpha \\ \hat{I}^\beta\end{pmatrix} = \begin{pmatrix}-\Gamma_\alpha - \frac{1}{T_1} + i\pi J & \frac{1}{T_1} \\ \frac{1}{T_1} & -\Gamma_\beta - \frac{1}{T_1} - i\pi J\end{pmatrix}\begin{pmatrix}\hat{I}^\alpha \\ \hat{I}^\beta\end{pmatrix}. \qquad [20]$$

$\hat{\hat{\Gamma}}$ denotes the rate matrix. The eigenvalues λ_1 and λ_2 of the matrix $\hat{\hat{\Gamma}}$ are

$$\lambda_{1/2} = -\left(\Gamma_\Sigma + \frac{1}{T_1}\right) \pm \sqrt{(i\pi J - \Gamma_\Delta)^2 + \left(\frac{1}{T_1}\right)^2}, \qquad [21]$$

with $\Gamma_\Sigma = \frac{1}{2}(\Gamma_\alpha + \Gamma_\beta)$ and $\Gamma_\Delta = \frac{1}{2}(\Gamma_\alpha - \Gamma_\beta)$. After separation of the real and imaginary parts, one obtains for the root expression, which is $(\lambda_1 - \lambda_2)/2$,

$$(\lambda_1 - \lambda_2)/2 = \sqrt{(i\pi J - \Gamma_\Delta)^2 + \left(\frac{1}{T_1}\right)^2} = \frac{1}{\sqrt{2}}\sqrt{\sqrt{(\pi J)^4 - 2(\pi J)^2\left(\frac{1}{T_1^2} - \Gamma_\Delta^2\right) + \left(\frac{1}{T_1^2} + \Gamma_\Delta^2\right)^2} + \left(\frac{1}{T_1^2} + \Gamma_\Delta^2 - (\pi J)^2\right)}$$
$$- \frac{i}{\sqrt{2}}\sqrt{\sqrt{(\pi J)^4 - 2(\pi J)^2\left(\frac{1}{T_1^2} - \Gamma_\Delta^2\right) + \left(\frac{1}{T_1^2} + \Gamma_\Delta^2\right)^2} - \left(\frac{1}{T_1^2} + \Gamma_\Delta^2 - (\pi J)^2\right)} = \frac{1}{2}\Gamma^c - \frac{i}{2}\Delta\Omega^{\alpha,\beta}. \qquad [22]$$

The real part contains the effective relaxation rate of line α and β, the imaginary part the influence on the relative line position. The effects are illustrated in Fig. 9 for an assumed cross-correlated relaxation rate of 20 Hz (a, c) and 5 Hz (b). The splitting of the two lines is due to the NH coupling which was assumed to be 90 Hz. Figure 8 shows that the cross-correlated relaxation rate is influenced by T_1 relaxation only for rates $R_1 = 1/T_1$ in the order of $\pi^1 J_{HN}$. This is independent of the assumed cross-correlation rate of 20 or 5 Hz, respectively (a, b). As the rate $R_1 = 1/T_1$ increases, the difference of the chemical shifts of the two signals of the doublet becomes smaller. Expansion of the root expression in Eq. [22] according to Taylor yields the eigenvalues

$$\lambda_1 = -\Gamma_\alpha - \frac{1}{T_1} \pm i\sqrt{(\pi J)^2 - \frac{1}{T_1^2}}$$

$$\lambda_2 = -\Gamma_\beta - \frac{1}{T_1} \pm i\sqrt{(\pi J)^2 - \frac{1}{T_1^2}}. \qquad [23]$$

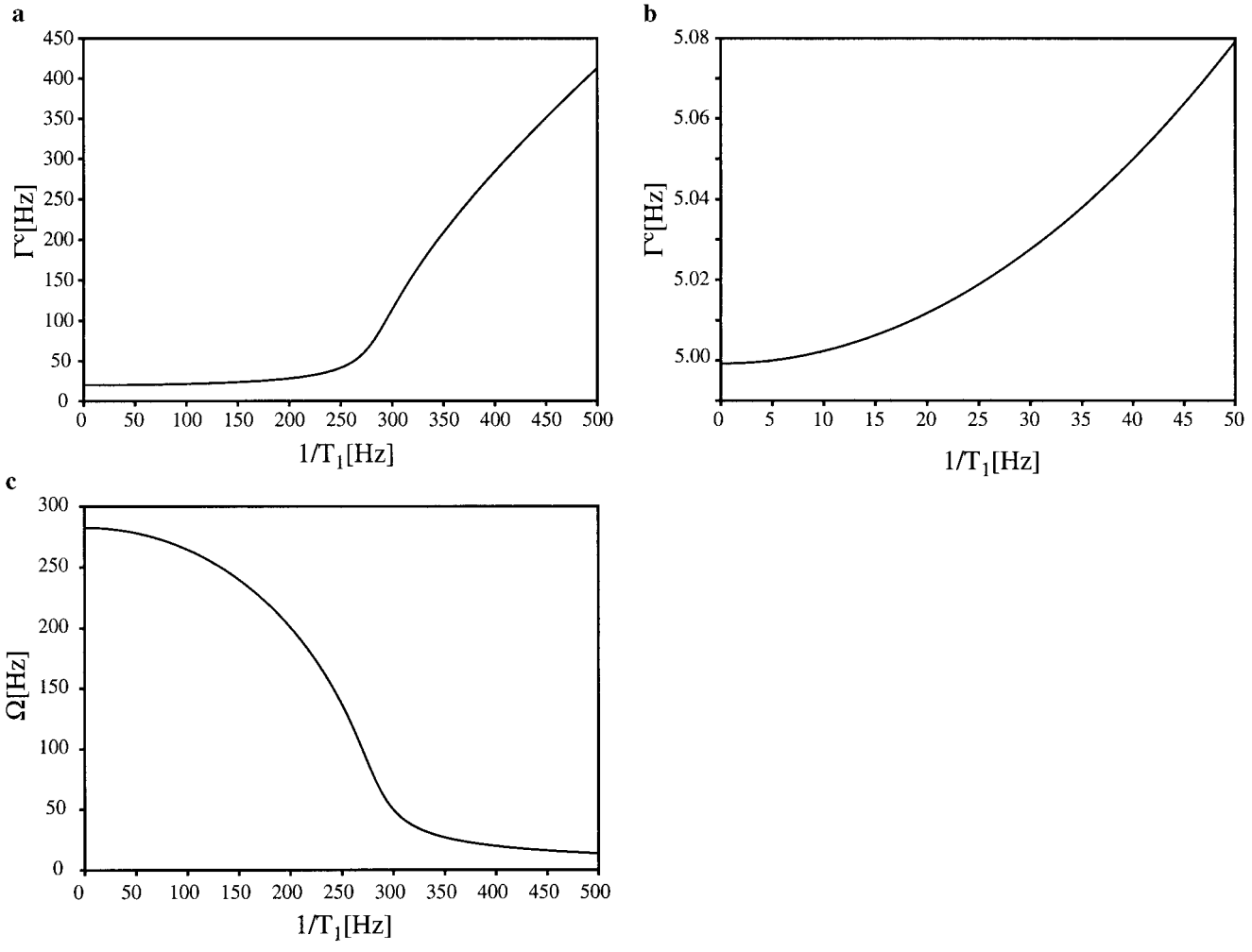

FIG. 9. Cross-correlated relaxation rate Γ^c of a doublet resonance line (a, b) and the relative chemical shift of one signal of the doublet (c) as a function of the proton T_1 time. The simulation is based on a cross-correlation rate of 20 Hz (a, c) and 5 Hz (b), respectively. The two resonance lines of the signal are split due to a scalar coupling of 90 Hz. The difference of real and imaginary part of the eigenvalues ($\lambda_1 - \lambda_2$) as obtained from Eq. [22] is shown. The real part corresponds to the cross-correlated relaxation rate, the imaginary part to the difference of chemical shift of the α- and β-component of the resonance line. The effects of dipole–dipole cross correlation are averaged out by the T_1 relaxation when the rate $1/T_1$ is in the order of the scalar coupling. In this case, however, the doublet is not resolved any more due to the decrease of α- and β-frequency difference $\Delta\Omega^{\alpha,\beta}$ with increasing rate $1/T_1$ (c).

Therefore, the dipole–dipole cross-correlated relaxation rate is independent of T_1 relaxation, as long as $\pi J \gg 1/T_1$.

EXPERIMENTAL IMPLEMENTATION

Introduction

The backbone angle ψ in proteins (Fig. 10) is relatively difficult to access by means of conventional NMR spectroscopic parameters. Either the scalar $^3J(H^N_{k+1}, C^\alpha_k)$ coupling (*21*) or the scalar $^3J(N_{k+1}, N_k)$ coupling (*22*), as well as distance measurements between the protons H^α_k and H^N_{k+1} (*23*) (Fig. 11b), turn out to be too inaccurate to define the angle properly. A different approach consists of the measurement of the relative displacements of the ^1H and ^{15}N resonance frequencies in 1:1 mixtures of D_2O and H_2O (*24*). It turns out that the solvent-induced chemical shift is a function of the backbone geometry around ψ. Recently, Yang *et al.* also suggested measuring the backbone angle ψ in a protein based on cross-correlated relaxation between the H^α–C^α dipolar and the C′ chemical shift anisotropy interaction mechanism (*25*).

The measurement of the parameter of cross-correlated relaxation rate of double- and zero-quantum coherences involving the two dipolar vectors C^α_k–H^α_k and N_{k+1}–H^N_{k+1} allows a quite accurate determination of the backbone angle ψ. This is shown in the following.

Correlation of θ and ψ, as shown in Fig. 11, reveals that

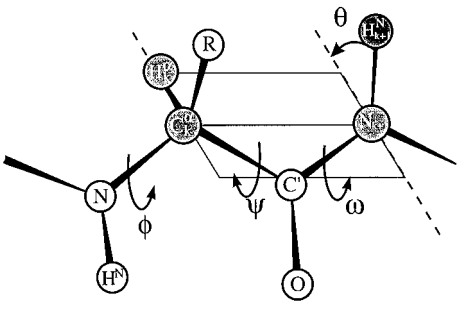

FIG. 10. Schematic representation of the peptide backbone with backbone angles ϕ, ψ, ω, and θ of amino acids k and $k+1$ in a protein. Assuming a planar backbone geometry, the measured angle θ can be correlated with the backbone angle ψ (see text). The plane which is spanned by the atoms H_k^α, C_k^α, and N_{k+1} is highlighted graphically.

regions of different secondary structure elements, as α-helices and β-sheets, can be differentiated. The $3\cos^2\theta - 1$ dependence of the cross-correlated relaxation is also not degenerate for the two secondary structure elements. The solid line $\cos(\theta) = 0.163 + 0.819 * \cos(\psi - 119°)$ can be obtained by means of geometrical considerations. Here bond lengths of $NH^N = 1.03$ Å, $C^\alpha H^\alpha = 1.09$ Å, $NC^\alpha = 1.47$ Å, $NC' = 1.33$ Å, and $C'C^\alpha = 1.52$ Å, as well as tetrahedral symmetry and the planarity of the peptide backbone, have been assumed.

Description of the Pulse Sequence and Experimental Results

The pulse sequence which is shown in Fig. 12 is essentially a HNCOCA-like experiment (*26*). A correlation between the two pairs of atoms C_k^α–H_k^α and N_{k+1}–H_{k+1}^N is achieved by excitation of double- and zero-quantum coherences during t_2. Starting from the proton H_{k+1}^N, magnetization is transferred to the nitrogen N_{k+1}. After a further INEPT transfer over C_k', magnetization is finally located on the carbon C_k^α. Through application of two simultaneous 90° pulses on ^{15}N and $^{13}C^\alpha$, DQ and ZQ coherences are excited for a constant time τ''. The delay τ'' is optimized with respect to the $C^\alpha C^\beta$ coupling.

Protons are not decoupled during t_2. Application of the pictographical analysis from the preceding section tells us that all cross-correlated relaxation rates, dipole/dipole as well as dipole/CSA, evolve during τ''. The experiment is symmetric around t_2. In the backtransfer step to the detected proton H_{k+1}^N, a COS-CT (coherence order selective coherence transfer) element is employed for optimal sensitivity.

For the design of pulse sequences that measure cross-correlated relaxation rates, pulse sequence elements affect the evolution under relaxation in a certain predictable way. This is quite different from autocorrelated relaxation where pulse sequence elements normally do not affect relaxation. This short section introduces some rules of calculation for how an effective Liouvillian can be calculated in a pulse sequence. Although several papers have been published on average Liouvillian theory (*27*), these simple rules have not been demonstrated so far.

Pulses of 180° allow us to manipulate the evolution of heteronuclear cross-correlated relaxation in a similar way as they allow us to manipulate the evolution of couplings and chemical shifts in heteronuclear spin systems. A train of 180°(^{1}H) is used, e.g., in ^{15}N relaxation measurements, to get rid of the dipole–CSA cross-correlated relaxation rates (*28*). The time evolution of the density matrix under the Hamilton operator and the relaxation superoperator is given by

$$\dot{\hat{\sigma}} = i[\hat{H}, \hat{\sigma}] - \hat{\hat{\Gamma}}(\hat{\sigma} - \hat{\sigma}_0). \qquad [24]$$

Ignoring the inhomogenous part and assuming weak coupling and the secular approximation for the relaxation superoperator we can treat the evolution under $\hat{\hat{\Gamma}}$ independently for each eigencoherence of the Hamiltonian $\hat{H}$:

$$\dot{\hat{\sigma}} = -\hat{\hat{\Gamma}}\hat{\sigma}. \qquad [25]$$

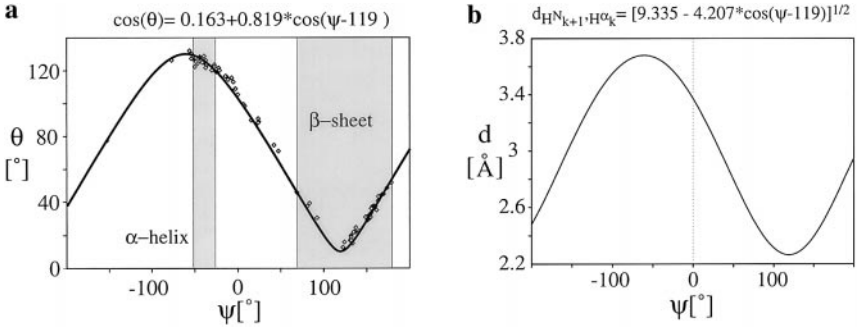

FIG. 11. (a) Correlation of the angles θ and ψ in the protein backbone from Fig. 10. Values of pairs of θ and ψ found for the protein rhodniin are depicted as diamonds (b) Distance between the H_{k+1}^N and the H_k^α proton as a function of the backbone angle ψ in a protein.

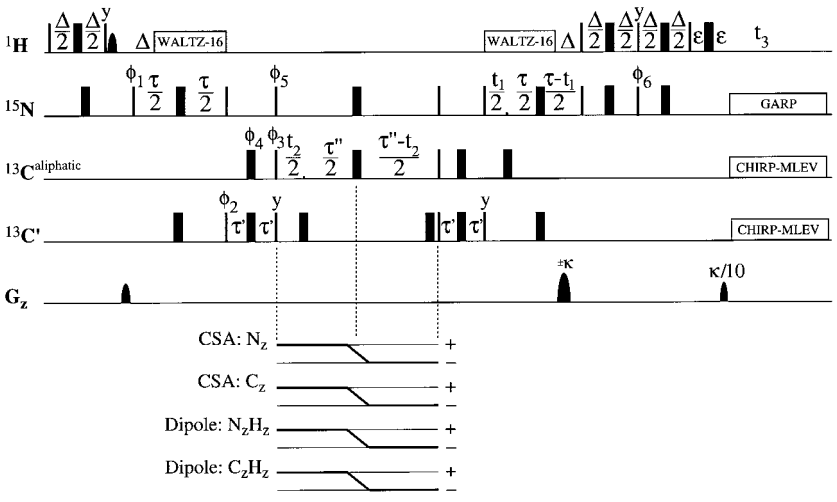

FIG. 12. HNCOCA-like pulse sequence for the measurement of N–H^N, C^α–H^α projection angles. DQ and ZQ coherences evolve chemical shift during t_1. Delays are as follows: $\Delta = 5$ ms, $\tau = 35$ ms, $2\tau' = 9$ ms, $\tau'' = 26$ ms, $\epsilon = 1.2$ ms. G3 and G4 Gaussian cascades (*31*) have been used as selective 90° and 180° pulses on C^α and C′ resonances. If not otherwise indicated, RF pulses have phase x. $\phi_1 = x, -x$; $\phi_2 = 2(x), 2(-x)$; $\phi_3 = 4(x), 4(-x)$; $\phi_5 = 8(x), 8(-x)$; $\phi_{rec} = \phi_1 + \phi_2 + \phi_3 + \phi_5$. Quadrature in t_2 is achieved by variation of phases ϕ_3 and ϕ_4 in States–TPPI manner. Echo–antiecho coherences are selected during t_1 by inversion of phases $\phi_6 = -y$ together with the sign of the second gradient (*32*). The phases ϕ_3 and ϕ_5 are shifted by 90° in subsequent FIDS and stored separately to be able to differentiate DQ and ZQ coherences during t_2. Aliphatic and carbonyl resonances are decoupled during acquisition using MLEV-expanded CHIRP pulses (*33*). Pictorial representation of the CSA and the dipolar coupling evolution. All interactions considered are inverted at $(\tau'' + t_2)/2$. Since the cross-correlated relaxation behaves like the product of the interaction that is cross correlated, $\Gamma_{CH,NH}$, $\Gamma_{N,NH}$, $\Gamma_{N,CH}$, $\Gamma_{C,CH}$, and $\Gamma_{C,NH}$ evolve during τ''.

Incorporation of a π-pulse in the pulse sequence leads to the equation of motion

$$(\hat{\hat{P}}\hat{\sigma})^{\cdot} = -\hat{\hat{\Gamma}}(\hat{\hat{P}}\hat{\sigma}). \qquad [26]$$

π-Pulses have the property that for many relaxation mechanisms either the commutator or the anticommutator vanishes.

$$[\hat{\hat{\Gamma}}, \hat{\hat{P}}] = \hat{\hat{\Gamma}}\hat{\hat{P}} - \hat{\hat{P}}\hat{\hat{\Gamma}} = 0 \quad \text{or} \quad [\hat{\hat{\Gamma}}, \hat{\hat{P}}]_+ = \hat{\hat{\Gamma}}\hat{\hat{P}} + \hat{\hat{P}}\hat{\hat{\Gamma}} = 0. \qquad [27]$$

In the first case, evolution of coherence under a certain relaxation is not affected by the π-pulse:

$$\hat{\hat{P}}\hat{\sigma}^{\cdot} = (\hat{\hat{P}}\hat{\sigma})^{\cdot} = -\hat{\hat{\Gamma}}\hat{\hat{P}}\hat{\sigma} = -\hat{\hat{P}}\,\hat{\hat{\Gamma}}\hat{\sigma}. \qquad [28]$$

In the second case, the sign of the evolution is changed:

$$\hat{\hat{P}}\hat{\sigma}^{\cdot} = (\hat{\hat{P}}\hat{\sigma})^{\cdot} = -\hat{\hat{\Gamma}}\hat{\hat{P}}\hat{\sigma} = +\hat{\hat{P}}\hat{\hat{\Gamma}}\hat{\sigma}. \qquad [29]$$

In this case, the π-pulse in the middle of two equal delays leads to refocusing of the effect of the relaxation mechanism. Since relaxation superoperators are derived from double commutators, we present some simple rules to easily see the effect of a π-pulse on a given relaxation rate. We assume we have two operators $\hat{A}$, $\hat{B}$, whose cross correlation is a source of relaxation. The relaxation superoperator is then given by

$$\hat{\hat{\Gamma}} = [\hat{A}, [\hat{B},]] + [\hat{A}^\dagger, [\hat{B}^\dagger,]].$$

A π-pulse on any coherence σ can be written as

$$\hat{\hat{P}}\hat{\sigma} = \hat{P}\hat{\sigma}\hat{P}^\dagger,$$

where $\hat{\hat{P}}$ is the superoperator effecting a π-rotation and $\hat{P}$ is the corresponding operator.

The two operators $\hat{A}$ and $\hat{B}$ shall be affected by the π-pulse in the following way:

TABLE 1
Tensor Operators in the Rotating Frame and Modified Spherical Harmonics for the Dipolar and CSA Interaction

	Tensor operators for the dipolar interaction $b_{kl} = -\mu_0 \frac{\gamma_k \gamma_l \hbar}{4\pi r_{kl}^3}$	Tensor operators for the CSA interaction $b_k = \frac{1}{3}(\sigma_\parallel - \sigma_\perp)\gamma_k B_0$	Modified spherical harmonics	Frequency
q	$\hat{A}_{kl}^{(q)}(\hat{I}_k, \hat{I}_l)$	$\hat{A}_k^{(q)}(\hat{I}_k)$	$F_k^{(q)}(\theta, \phi)$, $F_{kl}^{(q)}(\theta, \phi)$	ω_q
-2	$\sqrt{\frac{3}{8}}\hat{I}_k^- \hat{I}_l^-$	—	$\sqrt{\frac{3}{2}}\sin^2\theta \exp(+2i\phi)$	$\omega(\hat{I}_k) + \omega(\hat{I}_l)$
-1	$\sqrt{\frac{3}{8}}\hat{I}_{k,z}\hat{I}_l^-$	—	$\sqrt{6}\sin\theta\cos\theta\exp(+i\phi)$	$\omega(\hat{I}_l)$
-1	$\sqrt{\frac{3}{8}}\hat{I}_k^- \hat{I}_{l,z}$	$\sqrt{\frac{3}{8}}\hat{I}_k^-$	$\sqrt{6}\sin\theta\cos\theta\exp(+i\phi)$	$\omega(\hat{I}_k)$
0	$\hat{I}_{k,z}\hat{I}_{l,z}$	$\hat{I}_{k,z}$	$3\cos^2\theta - 1$	0
0	$-\frac{1}{4}(\hat{I}_k^+\hat{I}_l^- + \hat{I}_k^-\hat{I}_l^+)$	—	$3\cos^2\theta - 1$	$\omega(\hat{I}_k) - \omega(\hat{I}_l)$
$+1$	$\sqrt{\frac{3}{8}}\hat{I}_k^+ I_{l,z}$	$\sqrt{\frac{3}{8}}I_k^+$	$\sqrt{6}\sin\theta\cos\theta\exp(-i\phi)$	$\omega(\hat{I}_k)$
$+1$	$\sqrt{\frac{3}{8}}\hat{I}_{k,z}\hat{I}_l^+$	—	$\sqrt{6}\sin\theta\cos\theta\exp(-i\phi)$	$\omega(\hat{I}_l)$
$+2$	$\sqrt{\frac{3}{8}}\hat{I}_k^+\hat{I}_l^+$	—	$\sqrt{\frac{3}{2}}\sin^2\theta\exp(-2i\phi)$	$\omega(\hat{I}_k) + \omega(\hat{I}_l)$

Note. The calibration has been chosen such that $\oint_{4\pi}^{1} F^{(q)}(\theta, \phi)F^{(-q)}(\theta, \phi)d(\cos\theta)d\phi = \frac{4}{5}$, independent of q.

$$\hat{\hat{P}}\hat{A} = s_A\hat{A},\ \hat{\hat{P}}\hat{B} = s_B\hat{B} \quad \text{or} \quad \hat{\hat{P}}\hat{A} = s_A\hat{A}^\dagger,\ \hat{\hat{P}}\hat{B} = s_B\hat{B}^\dagger, \tag{30}$$

with s_A, $s_B = \pm 1$. These equations are true for all operators of Table 1 except for the case discussed below. Then it follows that

$$\hat{\hat{\Gamma}}\hat{\hat{P}}\hat{\sigma} = s_A s_B \hat{\hat{P}}\hat{\hat{\Gamma}}\hat{\sigma}. \tag{31}$$

Thus, if $s_A s_B = 1$ we have $[\hat{\hat{\Gamma}}, \hat{\hat{P}}] = 0$ and if $s_A s_B = -1$ we have $[\hat{\hat{\Gamma}}, \hat{\hat{P}}]_+ = 0$. An example to illustrate the commutator relations is described in Appendix 3.

Thus, it is sufficient to know whether the π-pulse inverts $\hat{A}$ ($s_A = -1$) or not ($s_A = 1$). The same holds for $\hat{B}$. We can pictorially represent the inversion of an interaction as depicted in Fig. 12 by drawing horizontal lines, the upper representing positive evolution of the operators $\hat{A}$ or $\hat{B}$ and the lower if it has been inverted. For a given cross-correlated relaxation rate, the sequence is segmented in the periods in which there is no sign change for $\hat{A}$ or for $\hat{B}$. Then the weighted sum over the times is formed with the weights being $s_A s_B$ for each time segment (Fig. 12).

In the autocorrelated case $s_A = s_B$ and therefore $s_A s_B = 1$. Therefore, autocorrelated relaxation is not affected by the application of a π-pulse and cannot be inverted by it. There is only one exception to this rule for the operators of Table 1 which is discussed in the appendixes. For the cross-correlated case, we consider here two examples.

(a) Dipole–dipole cross-correlated relaxation.

$$\hat{\hat{\Gamma}} = [\mathrm{H}_z^{\mathrm{N}}\mathrm{N}_z, [\mathrm{H}_z^{\mathrm{C}}\mathrm{C}_z,]] \tag{32}$$

Application of a $\pi(^{15}\mathrm{N})$-pulse or a $\pi(^{13}\mathrm{C})$-pulse leads to $s_A s_B = -1$ and therefore refocusing of the cross-correlated relaxation. A $\pi(^1\mathrm{H})$-pulse, however, does not affect the relaxation since $s_A s_B = +1$. This is used in the sequence of Fig. 12 where the $\pi(^{15}\mathrm{N})$-pulse and $\pi(^{13}\mathrm{C})$-pulse leave the HN, CH dipolar cross-correlated relaxation invariant.

(b) CSA–dipole cross-correlated relaxation.

$$\hat{\hat{\Gamma}} = [\sqrt{\tfrac{3}{8}}\,N^{+}, [\sqrt{\tfrac{3}{8}}\,H_z^N N^{-},]] + [\sqrt{\tfrac{3}{8}}\,N^{-}, [\sqrt{\tfrac{3}{8}}\,H_z^N N^{+},]] + [N_z, [H_z^N N_z,]] \qquad [33]$$

Application of a $\pi(^{15}N)$-pulse or a $\pi(^{13}C)$-pulse leads to $s_A s_B = +1$,

$$\hat{P} N^{-} = N^{-\dagger} = N^{+},$$

whereas a $\pi(^{1}H)$-pulse leads to refocusing of the interaction ($s_A s_B = -1$).

The pictorial representation used in Fig. 12 depicts the evolution of each of the Hamiltonians of interest during the period τ''. All operators are inverted after $(\tau'' + t_2)/2$ leading to the full evolution of all cross-correlated relaxation rates that originate from any of the magnetic interactions.

The DQ/ZQ HNCOCA experiment has been applied to the protein rhodniin which is a thrombin inhibitor. The protein consists of 103 amino acids and folds into two domains which are connected via a flexible linker. Each domain contains a triple-stranded β-sheet and a α-helical region. Experimentally obtained spectra are shown in Fig. 13. The doublet of doublet lines is not completely symmetric with respect to the resonance frequency. This is due to a different X–CSA contribution which can be observed on the multiplet lines correlated with the $^{1}J_{HX}$ coupling ($X = C^{\alpha}$ or N, respectively).

The cross-correlated relaxation rates $\Gamma^{c}_{NH,CH}$ can be extracted from the intensities of the lines $\alpha\alpha$, $\alpha\beta$, $\beta\alpha$, and $\beta\beta$ with the procedure described above.

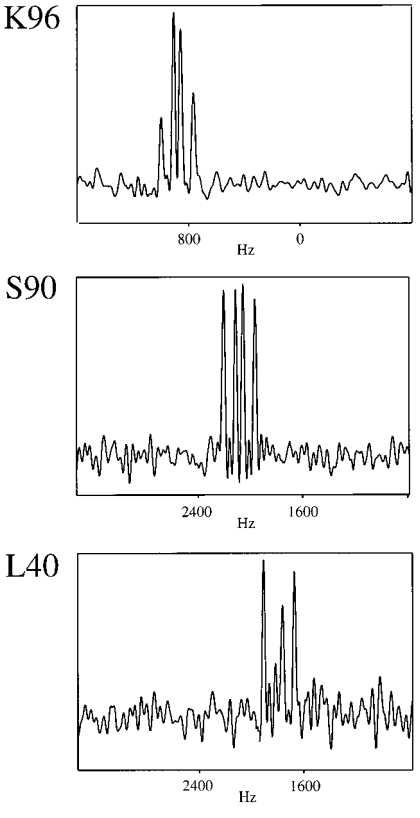

FIG. 13. 1D strips from the 3D DQ/ZQ HNCOCA for the residues K96, S90, and L40 in rhodniin corresponding to backbone angles ψ_{k-1}.

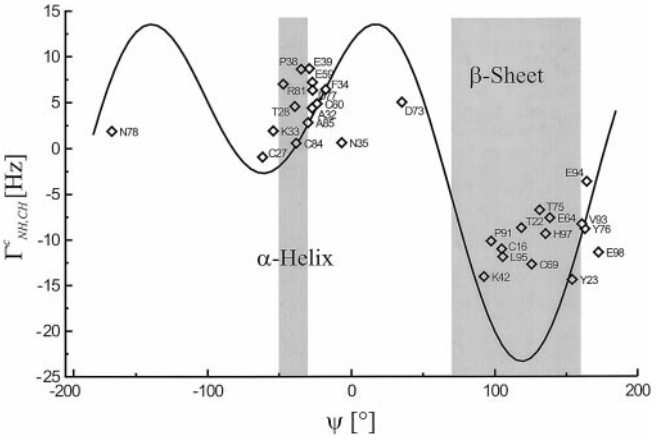

FIG. 14. Graphical representation of the extracted dipole$(NH)_{k+1}$–dipole$(CH)_k$ cross-correlated relaxation rates as a function of the backbone angle ψ_k as found from structure calculations before refinement. The solid line corresponds to Eq. [16]: $\Gamma^{c}_{NH,CH} + \frac{1}{2}(W_2 - W_0)$ as obtained with WTEST for a correlation time $\tau_c = 6.0$ ns.

Cross-Correlated Relaxation Rates as a Tool for Structure Refinement in Restrained MD Simulations

a. Dipole(^{15}N–$^{1}H^{N}$)–Dipole($^{13}C^{\alpha}$–$^{1}H^{\alpha}$). The extracted cross-correlated relaxation rates are used as restraints in the X-PLOR protocol to refine the backbone angle ψ. The starting structures for the Γ-refinement have been generated using the simulated annealing protocol developed by Brünger for X-PLOR (*29*). It consists of a 32.5-ps high-temperature phase at 2000 K, a first 25-ps cooling phase to 1000 K, and a second 10-ps cooling phase to a final temperature of 100 K. A total of 1645 unambiguous and 65 ambiguous NOE restraints have been taken into account as well as 22 dihedral restraints for the ϕ- and 28 dihedral restraints for the χ_1-angles. In addition, 34 hydrogen bonds have been identified by slow proton exchange of which 16 hydrogen bonds are implemented as ambiguous. The 30 structures with the lowest total energy out of 200 structures are chosen for further refinement. The average ψ-angles for the unrefined structures are shown in Fig. 14 together with $\Gamma^{c}_{NH,CH}$ as a function of ψ.

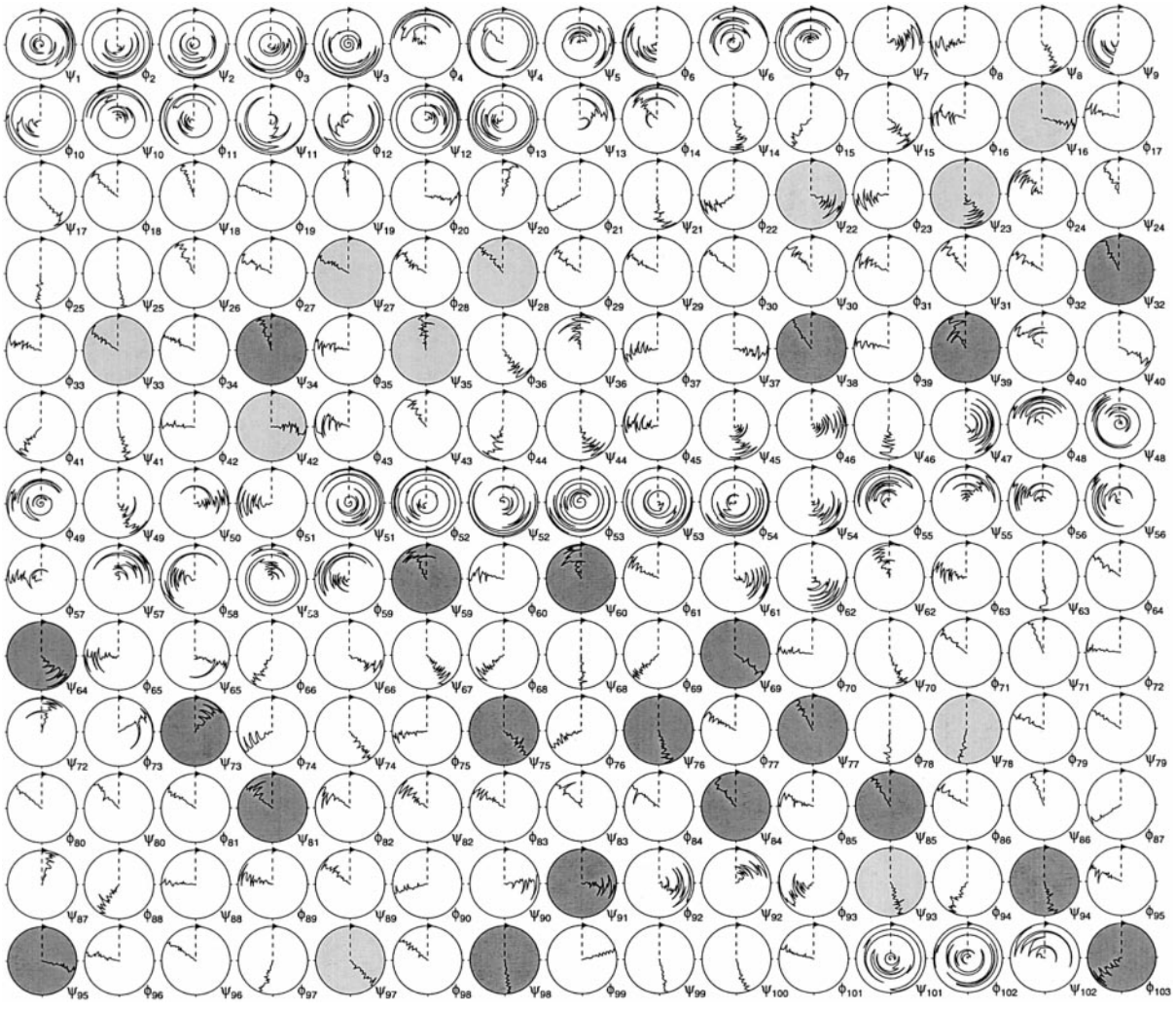

FIG. 15. Circle diagrams of the ϕ- and ψ-angles of all 30 structures before refinement. Shaded in light gray are all angles which will be restrained by $\Gamma^{c}_{CH,NH}$ relaxation rates; shaded in darker gray are all angles which will be additionally restrained by dipole–CSA relaxation rates in a second calculation. All circle diagrams in this paper have been prepared with the program MOLMOL (*34*).

Dipole(NH)–dipole(CH) cross-correlation rates tend to assume positive values for β-sheet regions, whereas they are around zero for α-helices. Coils and turns show negative rates. The theoretical angle-dependent cross-correlation rate is drawn with a solid line in Fig. 14. The curve was simulated with the program WTEST (*11*) assuming an overall correlation time of the molecule of $\tau_c = 6.0$ ns. This value is consistent with ^{15}N relaxation measurements (*30*) that yield a value of 6.4 ns for the second domain and a value of 5.4 ns for the first domain in rhodniin. In Fig. 15 the ϕ- and ψ-angles of all 30 unrefined structures are depicted in circle diagrams as obtained from MOLMOL. The count for the structures is encoded in the radius. Thus a straight line from the center of the circle to the diameter like for ψ_{38} indicates that the same value is obtained for all 30 structures. The dashed line indicates 0 for the angular value; the values increase clockwise. Shaded in light gray are angles restrained by dipole–dipole relaxation rates; shaded in darker gray are angles which will be additionally restrained by dipole–CSA relaxation rates in a further calculation.

The refinement is performed by a 100-ps restrained MD with all restraints included which have already been used in the simulated annealing plus 30 dipole–dipole cross-correlated relaxation rates. Since the dependence of the relaxation rate on the ψ-angle can be approximated by a Karplus-like function of the form $\Gamma^{c}_{ij}(\psi) = 25.536 \cos^2(\psi - 119°) + 10.332 \cos(\psi - 119°) - 12.309$ for $\tau_c = 6$ ns, the additional energy term is accounted for by making use of the parabolic potential for coupling constant refinement already implemented in

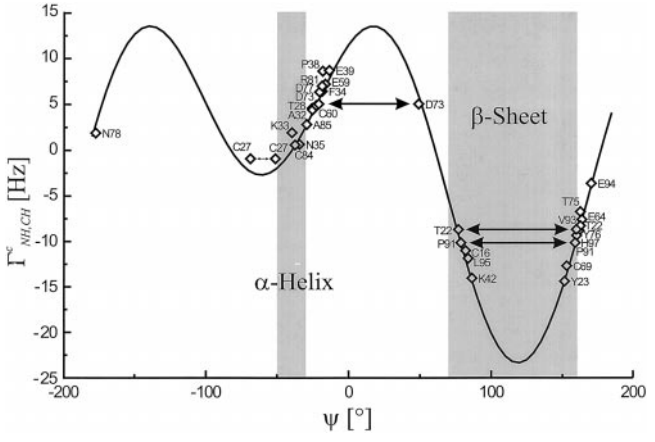

FIG. 16. Graphical representation of the extracted dipole$(NH)_{k+1}$–dipole$(CH)_k$ cross-correlated relaxation rates as a function of the backbone angle ψ_k as found from structure calculations after refinement with $\Gamma^c_{CH,NH}$ dipole–dipole relaxation rates.

X-PLOR. During the run, the force constant for the Γ-restraints is increased exponentially with time. Several calculations have been carried out using different final force constants. The force constants for the Γ-restraints were optimized such that the standard deviation of the calculated relaxation rates reflects their approximate experimental error. Thus, 1.25 kcal mol^{-1} Hz^{-2} turned out to be a reasonable value for the final force constant. Variation of the Γ error (which is defined in the same way as the *J*-error in the X-PLOR help function (29)) between 0 and 5 Hz did not have any effect on the results either for the regions with secondary structure or the loops except for a lower energy, the larger the Γ error was.

Figure 16 shows the experimental cross-correlation rates $\Gamma^c_{NH,CH}$ together with the respective average ψ-angles after this refinement procedure.

The rms difference for the relaxation rates to the experimental value decreases from 7.87 Hz for the starting structures to 0.97 Hz for the final structures. The average energy of the Γ-restraints drops from 2167.2 to 11.4 kcal/mol; the total energy rises from 663.9 kcal/mol for the protein without Γ-restraints to 833.9 kcal/mol for the restrained protein. For one restraint there are four and for another restraint there are three violations larger than 3 Hz in 30 structures. There are no violations larger than 5 Hz in any of the structures. The average standard deviation to the mean calculated relaxation rates amounts to 0.42 Hz. Most of the ψ-angles converge to a single value except those of the residues T22, C27, D73, and P91, which converge to two different values ($\psi^1_{22} = +77.0°$, $\psi^2_{22} = +159.9°$; $\psi^1_{27} = -68.5°$, $\psi^2_{27} = -51.1°$; $\psi^1_{73} = +49.2°$, $\psi^2_{73} = -20.9°$; $\psi^1_{91} = +78.7°$, $\psi^2_{91} = +159.0°$). To illustrate this effect, we have chosen the circle representation in Fig. 17. Shaded in light gray are all restrained angles; shaded in darker gray are the four angles with two different values.

Due to the refinement, the rms difference for the NOE restraints rises from 4.47×10^{-2} to 5.06×10^{-2} Å. The average rmsd value to the mean structure for the backbone atoms rises from 0.39 Å to 0.46 Å for the core region of the first domain (amino acids 14 to 48) and from 0.34 to 0.43 Å for the core region of the second domain (amino acids 66 to 101).

b. CSA(^{15}N)–Dipole($^{13}C^\alpha$–$^1H^\alpha$). Similar to a Karplus relation, the $3\cos^2\theta - 1$ function of the cross-correlated relaxation rate can also assume different ψ-values for one single cross-correlation rate. The main axis of the ^{15}N CSA tensor does not lie parallel to the N–H bond. Therefore, the cross-correlated relaxation rate $\Gamma^c_{N,CH}$ between the $(C^\alpha–H^\alpha)_k$ vector and the N_{k+1} CSA tensor has a different ψ-dependence than $\Gamma^c_{NH,CH}$ and can help to resolve the ψ-ambiguities (Fig. 18).

Figure 19 shows the dipole$(C^\alpha H^\alpha)_k$–CSA$(N)_{k+1}$ cross-correlated relaxation rate $\Gamma^c_{N,CH}$ as a function of the backbone angle ψ_k as found in structures calculated with X-PLOR before the refinement procedure.

The dependence of the CSA–dipole relaxation rate can be fitted in the same way as that of the dipole–dipole relaxation rate by a Karplus-like function. Here, one finds $\Gamma^c_{N,CH}(\psi) = 10.042\cos^2(\psi - 119°) + 7.971\cos(\psi - 119°) - 7.506$ for $\tau_c = 6$ ns. As the maximum value of the CSA–dipole relaxation rate is approximately half as large as the maximum value of the dipole–dipole relaxation rate, the force constant of the former is chosen four times as large as the force constant of the latter to achieve a roughly equal weight of both classes of restraints. If one uses all 33 measured CSA–dipole relaxation rates, some of them come into conflict with the dipole–dipole relaxation rates. This could be due to the fact that one measures the average relaxation rate of different conformations. Those can only be treated correctly by a refinement with ensemble-averaged cross-correlated restraints which will be left to further work. For the present calculations, all conflicting Γ-restraints were excluded so that one is left with 30 dipole–dipole and 19 CSA–dipole restraints. As in the calculations with dipole–dipole restraints only, the ψ-angles of residues T22, C27, and P91 converge to two different values ($\psi^1_{22} = +77.1°$, $\psi^2_{22} = +160.2°$; $\psi^1_{27} = -69.6°$, $\psi^2_{27} = -50.8°$; $\psi^1_{91} = +74.4°$, $\psi^2_{91} = +161.1°$). The relation of populated conformations of ψ_{73} shifts from 22:8 for $\psi^1_{73} = +49.2°$, $\psi^2_{73} = -20.9°$ to 27:3 for $\psi^1_{73} = +47.9°$, $\psi^2_{73} = -30.0°$. Hence, this is a case where the dipole–CSA restraints resolve an ambiguity found with dipole–dipole restraints alone. The values of the angles remain nearly unchanged compared to the calculations without dipole–CSA restraints. The dipole–dipole relaxation rates after the refinement are shown in Fig. 20; the dipole–CSA relaxation rates are shown in Fig. 21.

The circle diagrams in Fig. 22 illustrate the changed behavior for angle ψ_{73}.

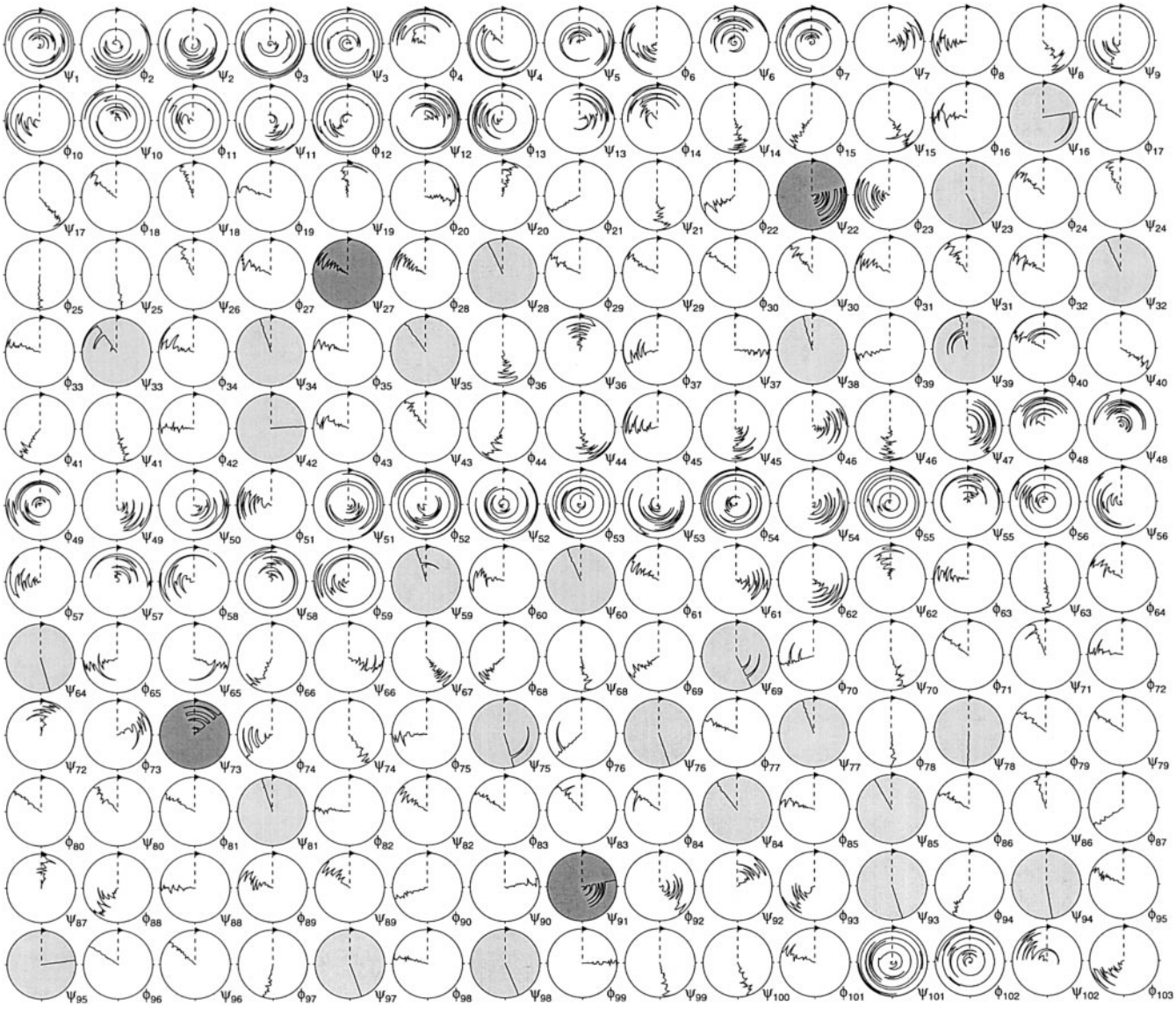

FIG. 17. Circle diagrams of the ϕ- and ψ-angles of all 30 structures after refinement with dipole–dipole relaxation rates. Shaded with light gray are all restrained angles; shaded with darker gray are the four angles which assume two values after refinement.

Due to the refinement, the rms difference of the Γ-restraints drops to 1.24 Hz with a standard deviation of 0.40 Hz for the dipole–dipole and of 0.16 Hz for the dipole–CSA restraints. There are no violations of the Γ-restraints larger than 5 Hz; two restraints are violated in 1 of 30 structures and one restraint is violated in 2 of 30 structures. During the refinement procedure, the total energy of the Γ-restraints decreases from 3113.7 to 140.4 kcal/mol. Nevertheless, the total energy rises compared to the unrefined protein from 663.9 to 979.2 kcal/mol. In part, the increase of the total energy is due to the fact that the limitation of the relaxation rates restrains the angles to a region smaller than the tolerance typically used for dihedral restraints of $\pm 30°$, so the entire structure is slightly more strained than without relaxation rate restraints. The rms difference for the NOE restraints rises to 5.13×10^{-2} Å. The average rmsd values to the mean structure for the backbone atoms rise from 0.39 to 0.46 Å for the core region of the first domain and from 0.34 to 0.42 Å for the core region of the second domain. Although the local rmsd has small maxima around amino acids with double ψ-angles, the rmsd is also increased for the other regions of the protein. The overall structure of the

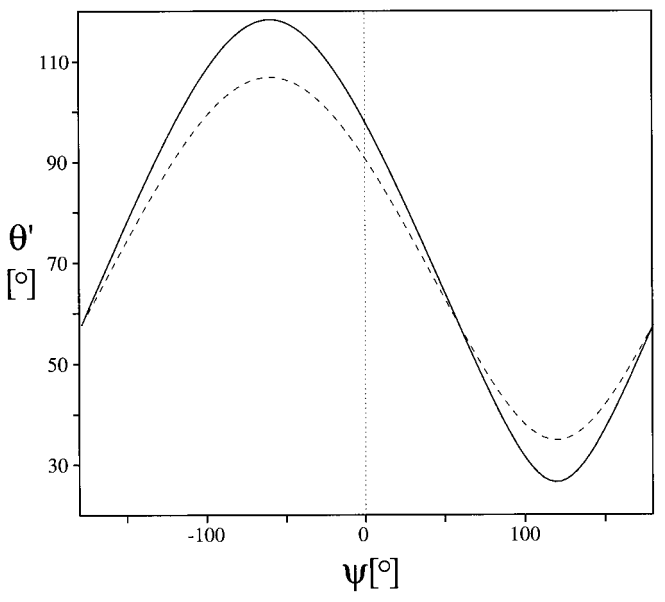

FIG. 18. $\theta'[(C^{\alpha}H^{\alpha})_k, \mathrm{CSA(N)}_{k+1}]$ as a function of the backbone angle ψ_k. The orientation of the CSA tensor is taken from solid-state NMR spectra (Ref. *14*). Values are taken from Hartzell *et al.* (*14b*) (solid line) giving $\theta' = \arccos[0.263 + 0.556*\cos(\psi - 119)]$ and Lumsden *et al.* (*14a*) (dashed line) giving $\theta' = \arccos[0.263 + 0.556*\cos(\psi - 119)]$.

protein does not change very much and its secondary structure is nearly unaffected by the refinement. The rmsd of the backbone atoms of the mean refined structure to the mean unrefined structure is 0.18 Å for the core region of the first domain and 0.31 Å for the core region of the second domain.

In principle, the cross-correlated relaxation rate $\Gamma^{c}_{N,NH}$ between the ^{15}N CSA tensor and the N–H^{N} vector as well as the cross correlation rate $\Gamma^{c}_{C,CH}$ between the $^{13}C^{\alpha}$ CSA tensor and the $C^{\alpha}H^{\alpha}$ vector can also be obtained. However, these rates can be measured more reliably by means of ^{15}N and $^{13}C^{\alpha}$ relaxation measurements and therefore are not given here.

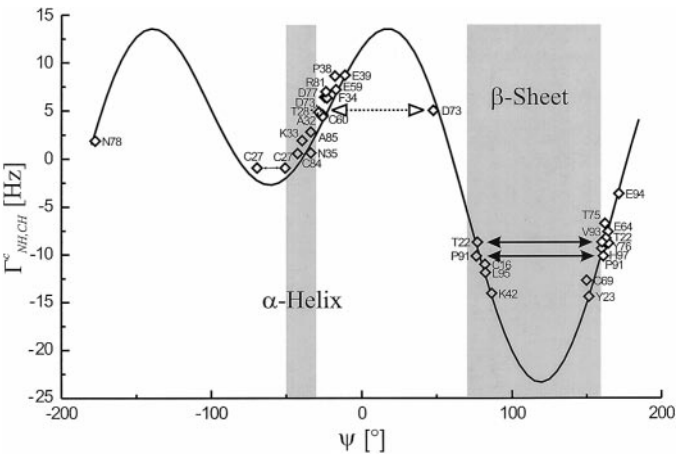

FIG. 20. Graphical representation of the extracted dipole$(NH)_{k+1}$–dipole$(CH)_k$ cross-correlated relaxation rates as a function of the backbone angle ψ_k as found after refinement with dipole–dipole and dipole–CSA relaxation rates. The dotted diamond gives the position of the only sparsely populated second conformation.

CONCLUSION

We have shown that cross-correlated relaxation rates, either between two dipolar or one dipolar and one CSA

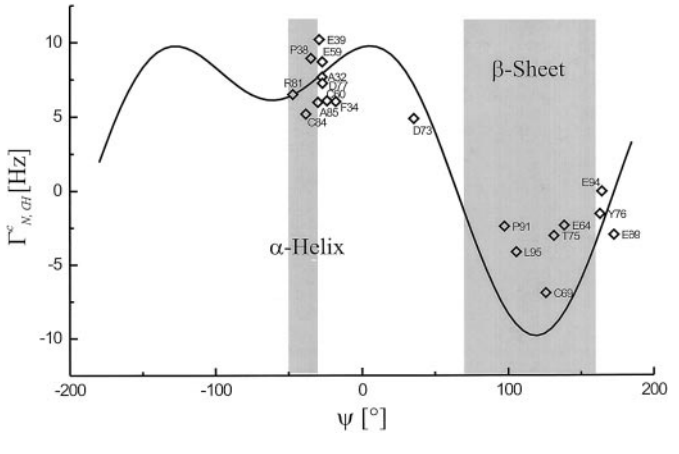

FIG. 19. Graphical representation of the extracted dipole$(C^{\alpha}H^{\alpha})_k$–$\mathrm{CSA(N)}_{k+1}$ cross-correlated relaxation rate $\Gamma^{c}_{N,CH}$ as a function of the mean backbone angle ψ_k of the unrefined structures.

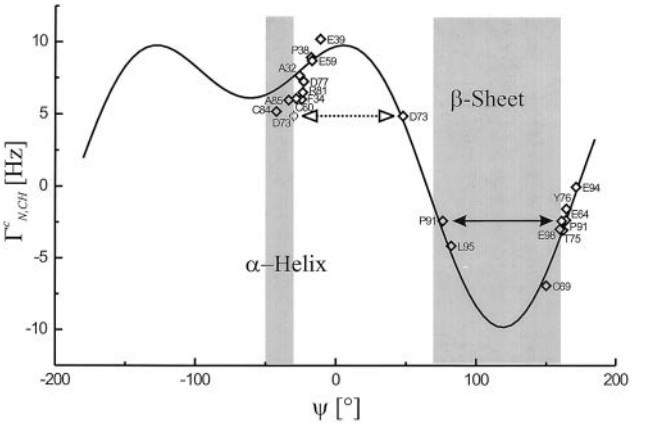

FIG. 21. Graphical representation of the extracted dipole$(C^{\alpha}H^{\alpha})_k$–$\mathrm{CSA(N)}_{k+1}$ cross-correlated relaxation rates as a function of the backbone angle ψ_k as found after refinement with dipole–dipole and dipole–CSA relaxation rates. The dotted diamond has the same meaning as in Fig. 20.

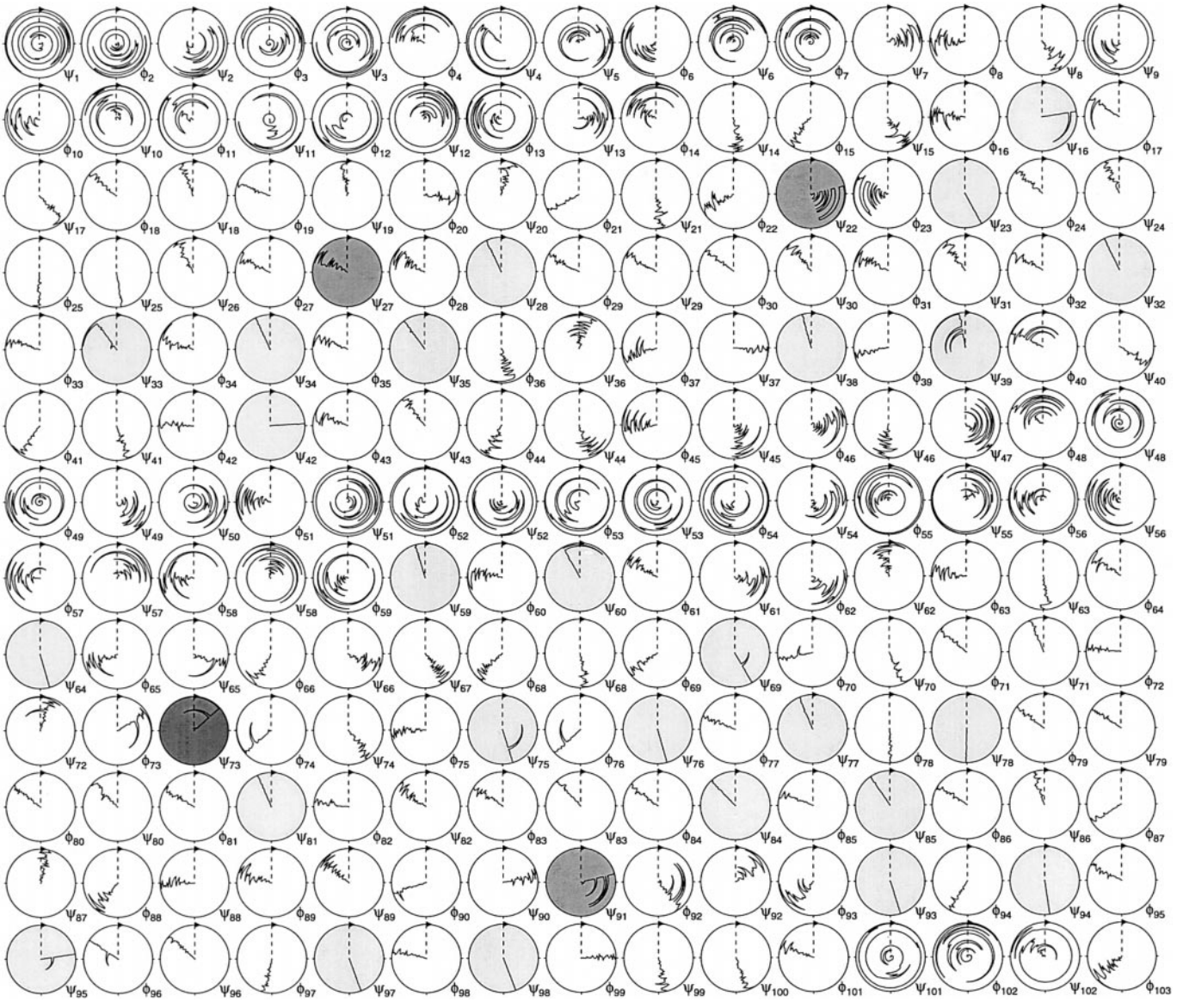

FIG. 22. Circle diagrams of the ϕ- and ψ-angles of all 30 structures after refinement with dipole–dipole and dipole–CSA relaxation rates. Shaded with light gray are all restrained angles; shaded with darker gray are the three angles which assume two values after refinement and shaded with dark gray is ψ_{73} which is restrained to a single value by additionally taking into account dipole–CSA relaxation rates.

interaction, can be used for the determination of the structure of a molecule by means of NMR. These new structural restraints are independent of any Karplus-type calibration and therefore are especially valuable for the conformational analysis of molecules where such a calibration is difficult to obtain. Furthermore, the effect of cross-correlated relaxation is not restrained to the analysis of local geometry, but can be used for the determination of the relative orientation between arbitrary directors within one molecule or between two molecules, if a correlation between these two can be established. Especially for, e.g., deuterated proteins or protein complexes, we expect this parameter to become a useful tool in the future.

APPENDIX 1

Hamilton Operators for the Dipole–Dipole and the Chemical Shift Anisotropy Interaction

A.1.1. Dipole–Dipole Interaction

The Hamiltonian describing the dipolar interaction between two spins can be written in the form (*12, 13, 19, 35*)

$$\hat{H}_{kl}^{\mathrm{DD}} = b_{kl}\left\{3\,\frac{1}{r_{kl}^2}\,(\hat{I}_k\mathbf{r}_{kl})(\hat{I}_l\mathbf{r}_{kl}) - \hat{I}_k\hat{I}_l\right\}$$

$$= b_{kl}\sum_{q=-2}^{+2} F_{kl}^{(q)}(\theta_{kl},\,\phi_{kl})\hat{A}_{kl}^{(q)}(\hat{I}_k,\,\hat{I}_l), \qquad [A1]$$

with

$$b_{kl} = -\mu_0\,\frac{\gamma_k\gamma_l\hbar}{4\pi r_{kl}^3}.$$

Thereby, γ_k and γ_l denote the gyromagnetic ratio of the nuclei k and l, $\hbar$ the Planck constant, and r the distance between the two nuclei. The angles θ_{kl}, ϕ_{kl} refer to the orientation of the vector $\mathbf{r}_{kl}$ with respect to the applied field. The exact expressions for the second-rank tensor operators $\hat{A}_{kl}^{(q)}(\hat{I}_k,\,\hat{I}_l)$ and the time-dependent modified spherical harmonics $F_{kl}^{(q)}(\theta_{kl},\,\phi_{kl})$ are given in Table 1.

The second main relaxation mechanism is relaxation through chemical shift anisotropy. The contribution to the Hamiltonian due to CSA in the principal axis frame (PAS) of nucleus k and in the laboratory frame (LF) can be written as (*12*, *13*, *19*, *35*)

$$\hat{H}_k^{\mathrm{CSA,PAS}} = \gamma_k\sum_{i=x,y,z} B_i\hat{\tilde{\sigma}}_{ii}^{k}\hat{I}_i^k \qquad [A.2a]$$

$$\hat{H}_k^{\mathrm{CSA,LF}} = b_k\sum_{q=-1}^{1} F_k^{(q)}(\theta_k,\,\phi_k)\hat{A}_k^{(q)}(\hat{I}_k), \qquad [A.2b]$$

with

$$b_k = \tfrac{1}{3}\,(\sigma_\parallel - \sigma_\perp)\gamma_k B_0$$

for axially symmetric CSA tensors. The B_i denote the components of the applied field B_0 in the PAS. In the LF, in analogy to Eq. [A.1], the CSA Hamiltonian can be separated into the time-dependent, orientational functions $F_k^{(q)}(\theta_k,\,\phi_k)$ and the time-independent spin operator terms $\hat{A}_k^{(q)}(\hat{I}_k)$ (*12*, *13*, *35*). The expressions for the second-rank tensor operators $\hat{A}_k^{(q)}(\hat{I}_k)$ and the time-dependent modified spherical harmonics $F_k^{(q)}(\theta_k,\,\phi_k)$ are again summarized in Table 1. The angles θ_k and ϕ_k are the polar coordinates of the main axis of the axially symmetric tensors in the laboratory frame.

The convention we use for $\hat{A}_k^{(q)}(\hat{I}_k)$ and $F_k^{(q)}(\theta_k,\,\phi_k)$ ensures that the integral

$$\frac{4}{5} = \frac{1}{4\pi}\oint F^{(q)}(\theta,\,\phi)\,F^{(-q)}(\theta,\,\phi)d(\cos\theta)d\phi$$

and therefore the spectral density functions

$$j^{(q)}(\omega_q) = \frac{4}{5}\,\frac{\tau_c}{1 + (\omega\tau_c)^2}$$

are independent of q.

For Eq. [A.2b], we assumed an axially symmetric tensor. However, this is no restriction of generality since each asymmetric CSA tensor can be decomposed into a superposition of two axially symmetric tensors: The bilinear form of the CSA contribution to the Hamilton operator in the PAS from Eq. [A.2] can be—after diagonalization of the CSA tensor—rewritten as (*35*)

$$\hat{H}_k^{\mathrm{CSA,PAS}} = \gamma_k\,\frac{\sigma_{xx} + \sigma_{yy} + \sigma_{zz}}{3}\,\mathbf{B}\hat{I}_k + \frac{1}{3}\,\gamma_k(\sigma_{xx} - \sigma_{zz})$$
$$\times\,[2\hat{I}_{k,x}B_x - \hat{I}_{k,y}B_y - \hat{I}_{k,z}B_z] + \frac{1}{3}\,\gamma_k(\sigma_{yy} - \sigma_{zz})$$
$$\times\,[2\hat{I}_{k,y}B_y - \hat{I}_{k,x}B_x - \hat{I}_{k,z}B_z]. \qquad [A.3]$$

The first term in Eq. [A.3] describes the isotropic part of the chemical shift, the second and third terms, the axially symmetric anisotropic contributions. Equation [A.3] can be used for the description of cross correlation between arbitrarily anisotropic tensors since an asymmetric anisotropic tensor of rank 2 can be contracted from two axially symmetric tensors lying along orthogonal axes. Using Table 1, $\sigma_\parallel - \sigma_\perp$ would be $\sigma_{xx} - \sigma_{zz}$ with x as axis of reference due to the second term, and $\sigma_\parallel - \sigma_\perp$ would be $\sigma_{yy} - \sigma_{zz}$ with y as axis of reference due to the third term in Eq. [A.3]. For the special case of a symmetric CSA tensor ($\sigma_{xx} = \sigma_{yy} = \sigma_\perp$), one finds

$$\hat{H}_k^{\mathrm{CSA,PAS}} = \gamma_k[\sigma_\parallel\hat{I}_{k,z}B_z + \sigma_\perp(\hat{I}_{k,x}B_x + \hat{I}_{k,y}B_y)]$$
$$= \gamma_k\left\{\frac{\sigma_\parallel + 2\sigma_\perp}{3}\,\mathbf{B}\hat{I}_k + \frac{\sigma_\parallel - \sigma_\perp}{3}\right.$$
$$\left.\times\,(2\hat{I}_{k,z}B_z - \hat{I}_{k,x}B_x - \hat{I}_{k,y}B_y)\right\}, \qquad [A.4]$$

with $\sigma_\parallel - \sigma_\perp = \sigma_{zz} - \frac{1}{2}(\sigma_{xx} + \sigma_{yy})$.

APPENDIX 2

Relaxation Superoperator and Spectral Density Functions

The relaxation superoperator in the Liouville–von Neumann equation,

$$\frac{d}{dt}\,\hat{\sigma} = -i[\hat{H}_0,\,\hat{\sigma}(t)] - \sum_{V,W}\hat{\tilde{\Gamma}}_{V,W}(\hat{\sigma}(t) - \hat{\sigma}(0)), \qquad [A.5]$$

has the general form

$$\hat{\hat{\Gamma}}_{VW}\hat{\sigma} = b_V b_W \sum_q [\hat{A}_V^{(-q)}, [\hat{A}_W^{(q)}, \hat{\sigma}]] * j_{VW}^q(\omega_q), \quad [A.6]$$

where the indices V and W refer to the interactions that are the source for relaxation. The term $j_{VW}^q(\omega_q)$ denotes the spectral density function and is obtained by evaluating the correlation function of the spherical harmonics,

$$j_{VW}^q(\omega_q) = \int_0^\infty d\tau \overline{F_V^{(q)}(t) F_W^{(-q)}(t+\tau)} \exp(-i\omega_q\tau). \quad [A.7]$$

The bar indicates time average over t. In the autocorrelation case ($V = W$), both interactions V and W are originating from the same source of interaction, e.g., the same pair of nuclei. In the cross-correlation case, the time-dependent spherical harmonics refer to different kinds of tensorial interactions ($V \neq W$).

The cross-correlation case only shall be considered in the following. The theory for the description of intramolecular dipolar interaction in coupled multispin systems has been developed some time ago (*36–40*). Formulae have been derived for the three cases of isotropic, axially symmetric, and generally anisotropic reorientation which are given in the following. A review on this topic is found in Ref. (*40*).

A.2.1. Spherical Top Molecules

The spectral density function for isotropic rotational diffusion has been derived by Hubbard and Kuhlmann and Baldeschweiler (*36a, 37*),

$$\begin{aligned} j_{VW}^q(\omega_q) &= \frac{2}{5}(3\cos^2\theta_{V,W} - 1)\left[\frac{6D}{(6D)^2 + \omega_q^2}\right] \\ &= \frac{1}{5}(3\cos^2\theta_{V,W} - 1)\left[\frac{2\tau_c}{1 + (\omega_q\tau_c)^2}\right]. \end{aligned} \quad [A.8]$$

D denotes the diffusion constant, with $1/\tau_c = 6D$. V and W denote the different interactions. $\theta_{V,W}$ describes the projection angle between the principal axes of the two interactions V and W. If V denotes, e.g., a N–H and W a C–H dipolar interaction, respectively, as indicated in Fig. 1, θ is the included angle between the two bond vectors N–H and C–H.

A.2.2. Asymmetric Top Molecules

The spectral density function for the asymmetric top assumes the form (*36c, 38, 40*)

$$\begin{aligned} j_{VW}^q(\omega_q) = \frac{1}{10} * \{ & 12\cos\theta_V\cos\theta_W\sin\theta_V\sin\theta_W\sin\phi_V\sin\phi_W \\ & \times \frac{b_1}{b_1^2 + \omega_q^2} + 12\cos\theta_V\cos\theta_W\sin\theta_V\sin\theta_W \\ & \times \cos\phi_V\cos\phi_W\frac{b_2}{b_2^2 + \omega_q^2} + 3\sin^2\theta_V \\ & \times \sin^2\theta_W\sin 2\phi_V\sin 2\phi_W \frac{b_3}{b_3^2 + \omega_q^2} \\ & + \left[3\cos^2\left(\frac{\zeta}{2}\right)\sin^2\theta_V\sin^2\theta_W\cos 2\phi_V\cos 2\phi_W \right. \\ & + \sin^2\left(\frac{\zeta}{2}\right)(3\cos^2\theta_V - 1)(3\cos^2\theta_W - 1) \\ & + \sqrt{3}\cos\left(\frac{\zeta}{2}\right)\sin\left(\frac{\zeta}{2}\right) \\ & \times ((3\cos^2\theta_V - 1)\sin^2\theta_W\cos 2\phi_W \\ & \left. + (3\cos^2\theta_W - 1)\sin^2\theta_V\cos 2\phi_V) \frac{b_4}{b_4^2 + \omega_q^2} \right. \\ & + \left[3\sin^2\left(\frac{\zeta}{2}\right)\sin^2\theta_V\sin^2\theta_W\cos 2\phi_V\cos 2\phi_W \right. \\ & + \cos^2\left(\frac{\zeta}{2}\right)(3\cos^2\theta_V - 1)(3\cos^2\theta_W - 1) \\ & - \sqrt{3}\cos\left(\frac{\zeta}{2}\right)\sin\left(\frac{\zeta}{2}\right)((3\cos^2\theta_V - 1) \\ & \times \sin^2\theta_W\cos 2\phi_W \\ & \left. + (3\cos^2\theta_W - 1)\sin^2\theta_V\cos 2\phi_V) \frac{b_5}{b_5^2 + \omega_q^2} \right\}, \end{aligned} \quad [A.9]$$

where the notation of Woessner (*41*) has been used:

$$D = \tfrac{1}{3}(D_{xx} + D_{yy} + D_{zz})$$

$$L^2 = \tfrac{1}{3}(D_{xx}D_{yy} + D_{xx}D_{zz} + D_{yy}D_{zz})$$

$$\tan\zeta = \sqrt{3}\left[\frac{D_{xx} - D_{yy}}{2D_{zz} - D_{xx} - D_{yy}}\right]$$

$$b_1 = 4D_{xx} + D_{yy} + D_{zz}$$

$$b_2 = D_{xx} + 4D_{yy} + D_{zz}$$

$$b_3 = D_{xx} + D_{yy} + 4D_{zz}$$

$$b_4 = 6D + 6\sqrt{D^2 - L^2}$$

$$b_5 = 6D - 6\sqrt{D^2 - L^2}. \qquad [A.10]$$

A.2.3. Axially Symmetric Top Molecules

For the case that $D_{xx} = D_{yy} = D_\perp$, Eq. [A.9] can be simplified yielding the spectral density function of the symmetric top rotator ($D_{zz} = D_\parallel$) (*36b, 42*).

$$\begin{aligned} j^q_{VW}(\omega_q) = \tfrac{1}{20}\{&(3\cos^2\theta_V - 1)(3\cos^2\theta_W - 1)\, J^{q,0}_{VW} \\ &+ 12\cos\theta_V\cos\theta_W\sin\theta_V\sin\theta_W \\ &\times \cos(\phi_V - \phi_W)\, J^{q,1}_{VW} \\ &+ 3\sin^2\theta_V\sin^2\theta_W\cos(2\phi_V - 2\phi_W)\, J^{q,2}_{VW}\}, \end{aligned} \qquad [A.11]$$

where the reduced spectral density functions ($-2 \le m \le +2$),

$$J^{q,m}_{VW} = \frac{2\tau_{c,m}}{1 + (\omega_q\tau_{c,m})^2}, \qquad [A.12]$$

have been used. The correlation times $\tau_{c,m}$ can be rewritten as diffusion constants $D_\parallel$ and $D_\perp$ according to

$$1/\tau_{c,m} = 6D_\perp + m^2(D_\parallel - D_\perp). \qquad [A.13]$$

A.2.4. Inclusion of Internal Motion

Internal motion can be incorporated into the spectral density either by the Lipari and Szabo (*43*) approach or by explicit calculation of the motion from, e.g., motional models of molecular dynamics trajectories. In Eq. [A.7], the spectral densities are Fourier transformations of the motion of the molecule with respect to the external magnetic field. This equation assumed that internal motion is absent. Rewriting the spectral densities as a convolution ($\times$) of a Fourier transformation of the global motion and the Fourier transformation of the local motion, we find for the first term $j^q_{V,W}(\omega_q)$ in Eq. [A.11] for axially symmetric diffusion:

$$\begin{aligned} j^{q,\text{local motion}}_{VW}(\omega_q) = &\tfrac{1}{5}\,FT \\ &\times \{\overline{P_2[\cos\theta_V(t)]P_2[\cos\theta_W(t+\tau)]} \times J^{q,0}_{VW}\}|_{\omega_q} + \cdots \end{aligned} \qquad [A.14]$$

The Fourier transformation concerns τ; the average is taken with respect to t. $P_2[\cos\theta]$ denotes the Legendre polynomials $(3\cos^2\theta - 1)/2$. If we assume the internal motion to be uncorrelated and fast with respect to the global motion, Eq. [A.14] can be directly used to compare field-dependent experimental relaxation rates with predicted rates and for the analysis of molecular dynamics trajectories or for the analysis of models.

Application of the Lipari and Szabo approach assumes in addition an exponential decay of the correlation function with the characteristic rate τ_i from time 0 to the time τ according to

$$\begin{aligned} &\overline{P_2[\cos\theta_V(t)]P_2[\cos\theta_W(t+\tau)]} \\ &= \exp\left(-\frac{\tau}{\tau_i}\right)\{\overline{P_2[\cos\theta_V(t)]P_2[\cos\theta_W(t)]} \\ &\quad - \overline{P_2[\cos\theta_V(t)]P_2[\cos\theta_W(t+\infty)]}\} \\ &\quad + \overline{P_2[\cos\theta_V(t)]P_2[\cos\theta_W(t+\infty)]} \\ &= \left\{\exp\left(-\frac{\tau}{\tau_i}\right)[1 - (S^{q,0}_{VW})^2] + (S^{q,0}_{VW})^2\right\} \\ &\quad \times \overline{P_2[\cos\theta_V(t)]P_2[\cos\theta_W(t)]}, \end{aligned} \qquad [A.15]$$

where $(S^{q,0}_{VW})^2$ is the order parameter for the respective interaction and τ_i corresponds to the internal correlation time (*44, 45*).

APPENDIX 3

Transformation Properties of Relaxation Superoperators under π-pulses

The transformation of the relaxation operators under π-pulses is described in Eq. [31]. There is, however, one exception to this rule for the operators of Table 1. A selective π-pulse on spin I_k applied to $\hat{A}^{(\pm 2)}_{kl}(\hat{I}_k, \hat{I}_l) = \sqrt{\tfrac{3}{8}}\hat{I}^\pm_k\hat{I}^\pm_l$ leads to $\hat{\hat{P}}_{k,x}\sqrt{\tfrac{3}{8}}\,\hat{I}^\pm_k\hat{I}^\pm_l = \sqrt{\tfrac{3}{8}}\,\hat{I}^\mp_k\hat{I}^\pm_l$. Conversely, $\hat{\hat{P}}_{k,x}\sqrt{\tfrac{3}{8}}\,\hat{I}^\mp_k\hat{I}^\pm_l = \sqrt{\tfrac{3}{8}}\,\hat{I}^\pm_k\hat{I}^\pm_l$. Thus these operators are not transformed into themselves or their hermitian conjugate. For example, we find for a relaxation superoperator,

$$\begin{aligned} \hat{\hat{\Gamma}}\hat{\hat{P}}_{k,x}\hat{\sigma} &= b_{kl}b_{kn}j^{(0)}(0)[-\tfrac{1}{4}(\hat{I}^+_k\hat{I}^-_l + \hat{I}^-_k\hat{I}^+_l), \\ &\qquad [-\tfrac{1}{4}(\hat{I}^+_k\hat{I}^-_n + \hat{I}^-_k\hat{I}^+_n), \hat{\hat{P}}_{k,x}\hat{\sigma}]] \\ &= b_{kl}b_{kn}j^{(0)}(0)\hat{\hat{P}}_{k,x}[-\tfrac{1}{4}(\hat{I}^-_k\hat{I}^-_l + \hat{I}^+_k\hat{I}^+_l), \\ &\qquad [-\tfrac{1}{4}(\hat{I}^-_k\hat{I}^-_n + \hat{I}^+_k\hat{I}^+_n),]] = \hat{\hat{P}}_{k,x}\hat{\hat{\Gamma}}'\hat{\sigma}. \end{aligned} \qquad [A.16]$$

Application to the NOESY experiment with a selective inversion pulse on spin I_k in the middle of a mixing time yields the transformation

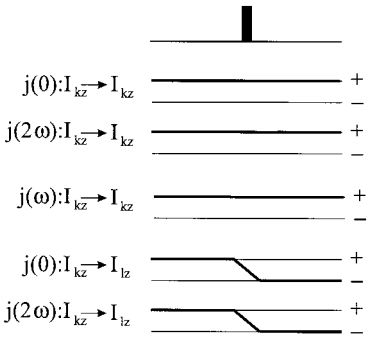

FIG. 23. Evolution under the relaxation superoperators of Eq. [A18]. An $\hat{I}_k$-selective inversion pulse leads to sign-inversion of the cross-relaxation rates originating from $j(0)$ and $j(2\omega)$ but not the eigenrelaxation rate.

$$\begin{aligned}\hat{\hat{\Gamma}}\hat{\hat{P}}_{k,x}\hat{I}_{kz} &= b_{kl}b_{kl}j^{(0)}(0)[-\tfrac{1}{4}(\hat{I}_k^+\hat{I}_l^- + \hat{I}_k^-\hat{I}_l^+),\\ &\quad [-\tfrac{1}{4}(\hat{I}_k^+\hat{I}_l^- + \hat{I}_k^-\hat{I}_l^+), \hat{\hat{P}}_{k,x}\hat{I}_{kz}]]\\ &= b_{kl}b_{kl}j^{(0)}(0)\hat{\hat{P}}_{k,x}[-\tfrac{1}{4}(\hat{I}_k^-\hat{I}_l^- + \hat{I}_k^+\hat{I}_l^+),\\ &\quad [-\tfrac{1}{4}(\hat{I}_k^-\hat{I}_l^- + \hat{I}_k^+\hat{I}_l^+), \hat{I}_{kz}] = \hat{\hat{P}}_{k,x}\hat{\hat{\Gamma}}'\hat{I}_{kz}. \quad [A.17]\end{aligned}$$

The double commutator yields

$$\begin{aligned}\hat{\hat{\Gamma}}\hat{I}_{kz} &= b_{kl}b_{kl}j^{(0)}(0)[-\tfrac{1}{4}(\hat{I}_k^+\hat{I}_l^- + \hat{I}_k^-\hat{I}_l^+),\\ &\quad [-\tfrac{1}{4}(\hat{I}_k^+\hat{I}_l^- + \hat{I}_k^-\hat{I}_l^+), \hat{I}_{kz}]]\\ &= b_{kl}b_{kl}j^{(0)}(0)(\hat{I}_{kz} - \hat{I}_{lz}) \qquad [A.18]\end{aligned}$$

and

$$\begin{aligned}\hat{\hat{\Gamma}}'\hat{I}_{kz} &= b_{kl}b_{kl}j^{(0)}(0)[-\tfrac{1}{4}(\hat{I}_k^-\hat{I}_l^- + \hat{I}_k^+\hat{I}_l^+),\\ &\quad [-\tfrac{1}{4}(\hat{I}_k^-\hat{I}_l^- + \hat{I}_k^+\hat{I}_l^+), \hat{I}_{kz}]]\\ &= b_{kl}b_{kl}j^{(0)}(0)(\hat{I}_{kz} + \hat{I}_{lz}).\end{aligned}$$

Thus we arrive at the well-known fact that the autocorrelated longitudinal eigenrelaxation of $\hat{I}_{kz}$ is not refocused by an $\hat{I}_k$-selective inversion pulse whereas cross relaxation $\hat{I}_{kz} \rightarrow \hat{I}_{lz}$ is suppressed (Fig. 23) (*46*).

ACKNOWLEDGMENTS

Support by the Fonds der Chemischen Industrie (A.D., M.H., M.M., C.G.) and the DFG (B.R.) is gratefully acknowledged. A.D. M. M., and M.H. are also supported by the Graduiertenkolleg: Chemische und Biologische Synthese von Wirkstoffen Grk 34/3. Continuous support by Dr. W. Bermel and Dr. T. Keller, Bruker Karlsruhe, is gratefully acknowledged. All measurements have been done at the Large Scale Facility for Biomolecular NMR at the University of Frankfurt. We thank Dr. T. Carlo Magno, Prof. Dr. S. J. Glaser, and Prof. Dr. H. J. Schwalbe for critical reading of the manuscript and valuable discussions.

REFERENCES

1. B. Reif, M. Hennig, and C. Griesinger, *Science* **276,** 1230–1233 (1997).
2. R. K. Hester, J. L. Ackermann, B. L. Neff, and J. S. Waugh, *Phys. Rev. Lett.* **36,** 1081 (1976); M. Linder, A. Höhener, and R. R. Ernst, *J. Chem. Phys.* **73,** 4959 (1980).
3. G. Dabbagh, D. P. Weli, and R. Tycko, *Macromolecules* **27,** 6183–6191 (1994).
4. K. Schmidt-Rohr, *Macromolecules,* **29,** 3975–3981 (1996); K. Schmidt-Rohr, *J. Am. Chem. Soc.* **118,** 7601–7603 (1996); X. Feng, Y. K. Lee, D. Sandström, M. Edén, H. Maisel, A. Sebald, and M. H. Levitt, *Chem. Phys. Lett.* **257,** 314–320 (1996); X. Feng, P. J. E. Verdegem, Y. K. Lee, D. Sandström, M. Edén, P. Bovee-Geurts, J. W. de Grip, J. Lugtenburg, H. J. M. de Groot, and M. H. Levitt, *J. Am. Chem. Soc.* **119,** 6853–6857 (1997); M. Hong, J. D. Gross, and R. G. Griffin, *J. Phys. Chem. B* **101,** 5869–5874 (1997).
5. C. Dalvit and G. Bodenhausen, *J. Am. Chem. Soc.* **110,** 7924 (1988).
6. R. Brüschweiler, C. Griesinger, and R. R. Ernst, *J. Am. Chem. Soc.* **111,** 8034 (1989).
7. R. L. Vold, R. R. Vold, and D. Canet, *J. Chem. Phys.* **66,** 1202 (1977); R. L. Vold and R. R. Vold, *Prog. NMR Spectrosc.* **12,** 79 (1978).
8. R. Freeman, S. Wittekoek, and R. R. Ernst, *J. Chem. Phys.* **52,** 1529 (1970); S. Schäublin, A. Höhener, and R. R. Ernst, *J. Magn. Reson.* **13,** 196 (1974).
9. M. Ernst and R. R. Ernst, *J. Magn. Reson. A* **110,** 202 (1994).
10. B. Brutscher, N. R. Skrynnikov, T. Bremi, R. Brüschweiler, and R. R. Ernst, *J. Magn. Reson.* **130,** 346 (1998).
11. Z. Madi and R. R. Ernst, "WTEST Program Package," Eidgenössische Technische Hochschule, Zürich (1989).
12. R. R. Ernst, G. Bodenhausen, and A. Wokaun, "Principles of Nuclear Magnetic Resonance in One and Two Dimensions," Clarendon Press, Oxford (1989).
13. J. Cavangh, W. J. Fairbrother, A. G. Palmer III, and N. J. Skelton, "Protein NMR Spectroscopy," Academic Press, San Diego (1996).
14. (a) M. D. Lumsden, R. W. Wasylishen, K. Eichele, M. Schindler, G. H. Penner, W. P. Power, and R. D. Curtis, *J. Am. Chem. Soc.* **116,** 1403 (1994); (b) C. J. Hartzell, M. Whitfield, T. G. Oas, and G. P. Drobny, *J. Am. Chem. Soc.* **109,** 5966 (1987).
15. N. Janes, S. Ganapathy, and E. Oldfield, *J. Magn. Reson.* **54,** 111 (1983).
16. T. M. Duncan, "A Compilation of Chemical Shift Anisotropies," Farragut, Chicago (1990).
17. C. Ye, R. Fu, J. Hu, Lei Hou, and S. Ding, *Magn. Reson. Chem.* **31,** 699–704 (1993).
18. B. Reif, H. Steinhagen, B. Junker, M. Reggelin, and C. Griesinger, *Angew. Chem.* **110,** 2006 (1998); *Angew. Chem. Int. Ed. Engl.* **37,** 1903–1906 (1998).
19. A. Abragam, "The Principles of Nuclear Magnetism," Clarendon Press, Oxford (1961).
20. G. S. Harbison, *J. Am. Chem. Soc.* **115,** 3026 (1993); T. J. Norwood, *J. Magn. Reson. A* **104,** 106 (1993).
21. A. C. Wang and A. Bax, *J. Am. Chem. Soc.* **117,** 1810 (1995).

22. F. Löhr and H. Rüterjans, *J. Magn. Reson.* **132,** 130 (1998); K. Theis, A. J. Dingley, A. Hoffmann, J. G. Omichinski, and S. Grzesiek, *J. Biomol. NMR* **10,** 403 (1997).
23. K. Wüthrich, "NMR of Proteins and Nucleic Acids," Wiley, New York (1986).
24. M. Ottiger and A. Bax, *J. Am. Chem. Soc.* **119,** 8070–8075 (1997).
25. D. Yang, R. Konrat, and L. E. Kay, *J. Am. Chem. Soc.* **119,** 11938–11940 (1997).
26. A. Bax and M. Ikura, *J. Biomol. NMR* **1,** 99 (1991).
27. J. Jeener, *Adv. Magn. Reson.* **10,** 1–51 (1982); S. A. Smith, W. E. Palke, and J. T. Gerig, *J. Magn. Reson. A* **106,** 57–64 (1994); M. H. Levitt and L. Di Bari, *Phys. Rev. Lett.* **69,** 3124–3127 (1992); M. H. Levitt and L. Di Bari, *Bull. Magn. Reson.* **16,** 94–114 (1994); P. Allard, M. Helgstrand, and T. Härd, *J. Magn. Reson.* **134,** 7–16 (1998); R. Ghose, T. R. Eykyn, and G. Bodenhausen, *Mol. Phys.* **96,** 1281–1288 (1999); E. Chiarparin, P. Pelupessy, R. Ghose, and G. Bodenhausen, *J. Am. Chem. Soc.* **121,** 6876–6883 (1999).
28. J. Boyd, L. Hommel, and I. D. Campbell, *Chem. Phys. Lett.* **175,** 477 (1990); D. Yang, K. H. Gardner, and L. E. Kay, *J. Biomol. NMR* **11,** 213 (1998).
29. A. T. Brünger, "X-PLOR Version 3.851: A System for X-Ray Crystallography and NMR," Yale Univ. Press, New Haven, CT (1992).
30. M. Hennig, "Diplomarbeit," Frankfurt/M. (1996).
31. L. Emsley and G. Bodenhausen, *J. Magn. Reson.* **82,** 211 (1989); L. Emsley and G. Bodenhausen, *Chem. Phys. Lett.* **165,** 469 (1989).
32. A. G. Palmer, J. Cavanagh, P. E. Wright, and M. Rance, *J. Magn. Reson.* **93,** 151 (1991); L. E. Kay, O. Keifer, and T. Saarinen, *J. Am. Chem. Soc.* **114,** 10663 (1992); J. Schleucher, M. Sattler, and C. Griesinger, *Angew. Chem. Int. Ed. Engl.* **32,** 1489 (1993); M. Sattler, M. G. Schwendinger, J. Schleucher, and C. Griesinger, *J. Biomol. NMR* **5,** 11 (1995).
33. R. Fu and G. Bodenhausen, *Chem. Phys. Lett.* **245,** 415 (1995).
34. R. Koradi, M. Billeter, and K. Wüthrich, *J. Mol. Graphics* **14,** 51 (1996).
35. M. Goldman, "Quantum Description of High-Resolution NMR in Liquids," Clarendon Press, Oxford (1988).
36. P. S. Hubbard, *Phys. Rev.* **109,** 1153 (1958); P. S. Hubbard, *J. Chem. Phys.* **51,** 1647 (1969); P. S. Hubbard, *J. Chem. Phys.* **52,** 563 (1970).
37. K. F. Kuhlmann and J. D. Baldeschweiler, *J. Chem. Phys.* **43,** 572 (1965).
38. H. Shimizu, *J. Chem. Phys.* **37,** 765 (1969).
39. D. M. Grant and L. G. Werbelow, *J. Magn. Reson.* **21,** 369 (1976).
40. L. G. Werbelow and D. M. Grant, *Adv. Magn. Reson.* **9,** 189 (1977).
41. D. E. Woessner, *J. Chem. Phys.* **36,** 1 (1962); D. E. Woessner, *J. Chem. Phys.* **37,** 647 (1962).
42. H. Schneider, *Z. Naturforsch. A* **19,** 510 (1964).
43. G. Lipari and A. J. Szabo, *J. Am. Chem. Soc.* **104,** 4546 (1982).
44. R. Brüschweiler and D. A. Case, *Prog. NMR Spectrosc.* **26,** 27 (1994).
45. B. Brutscher, N. R. Skrynnikov, T. Bremi, R. Brüschweiler, and R. R. Ernst, *J. Magn. Reson.* **130,** 346 (1998).
46. C. Zwahlen, S. J. F. Vincent, L. Di Bari, M. H. Levitt, and G. Bodenhausen, *J. Am. Chem. Soc.* **116,** 362 (1994); C. G. Hoogstraten, W. M. Westler, E. S. Mooberry, S. Macura, and J. L. Markley, *J. Magn. Reson. B* **109,** 76 (1995); C. G. Hoogstraten, S. Choe, W. M. Westler, and J. L. Markley, *Protein Sci.* **4,** 2289 (1995).